Universidade Federal de Goiás
Instituto de Física

Flávio Bento de Oliveira

Structural and electronic properties of functionalized germanene

Goiânia
2020

UNIVERSIDADE FEDERAL DE GOIÁS
INSTITUTO DE FÍSICA

TERMO DE CIÊNCIA E DE AUTORIZAÇÃO (TECA) PARA DISPONIBILIZAR VERSÕES ELETRÔNICAS DE TESES

E DISSERTAÇÕES NA BIBLIOTECA DIGITAL DA UFG

Na qualidade de titular dos direitos de autor, autorizo a Universidade Federal de Goiás (UFG) a disponibilizar, gratuitamente, por meio da Biblioteca Digital de Teses e Dissertações (BDTD/UFG), regulamentada pela Resolução CEPEC nº 832/2007, sem ressarcimento dos direitos autorais, de acordo com a Lei 9.610/98, o documento conforme permissões assinaladas abaixo, para fins de leitura, impressão e/ou download, a título de divulgação da produção científica brasileira, a partir desta data.

O conteúdo das Teses e Dissertações disponibilizado na BDTD/UFG é de responsabilidade exclusiva do autor. Ao encaminhar o produto final, o autor(a) e o(a) orientador(a) firmam o compromisso de que o trabalho não contém nenhuma violação de quaisquer direitos autorais ou outro direito de terceiros.

1. Identificação do material bibliográfico

[X] Dissertação [ ] Tese

2. Nome completo do autor

Flávio Bento de Oliveira

3. Título do trabalho

Structural and electronic properties of functionalized germanene

4. Informações de acesso ao documento (este campo deve ser preenchido pelo orientador)

Concorda com a liberação total do documento [ ] SIM [X] NÃO[1]

[1] Neste caso o documento será embargado por até um ano a partir da data de defesa. Após esse período, a possível disponibilização ocorrerá apenas mediante:
a) consulta ao(à) autor(a) e ao(à) orientador(a);
b) novo Termo de Ciência e de Autorização (TECA) assinado e inserido no arquivo da tese ou dissertação.
O documento não será disponibilizado durante o período de embargo.
Casos de embargo:
- Solicitação de registro de patente;
- Submissão de artigo em revista científica;
- Publicação como capítulo de livro;
- Publicação da dissertação/tese em livro.

Obs. Este termo deverá ser assinado no SEI pelo orientador e pelo autor.

Documento assinado eletronicamente por **FLÁVIO BENTO DE OLIVEIRA**, **Discente**, em 11/09/2020, às 15:08, conforme horário oficial de Brasília, com fundamento no art. 6º, § 1º, do Decreto nº 8.539, de 8 de outubro de 2015.

Documento assinado eletronicamente por **Andréia Luisa Da Rosa**, **Professor do Magistério Superior**, em 11/09/2020, às 16:47, conforme horário oficial de Brasília, com fundamento no art. 6º, § 1º, do Decreto nº 8.539, de 8 de outubro de 2015.

Processo: 23070.022664/2020-53 Documento: 3394617

UNIVERSIDADE FEDERAL DE GOIÁS
INSTITUTO DE FÍSICA

TERMO DE CIÊNCIA E DE AUTORIZAÇÃO (TECA) PARA DISPONIBILIZAR VERSÕES ELETRÔNICAS DE TESES

E DISSERTAÇÕES NA BIBLIOTECA DIGITAL DA UFG

Na qualidade de titular dos direitos de autor, autorizo a Universidade Federal de Goiás (UFG) a disponibilizar, gratuitamente, por meio da Biblioteca Digital de Teses e Dissertações (BDTD/UFG), regulamentada pela Resolução CEPEC nº 832/2007, sem ressarcimento dos direitos autorais, de acordo com a Lei 9.610/98, o documento conforme permissões assinaladas abaixo, para fins de leitura, impressão e/ou download, a título de divulgação da produção científica brasileira, a partir desta data.

O conteúdo das Teses e Dissertações disponibilizado na BDTD/UFG é de responsabilidade exclusiva do autor. Ao encaminhar o produto final, o autor(a) e o(a) orientador(a) firmam o compromisso de que o trabalho não contém nenhuma violação de quaisquer direitos autorais ou outro direito de terceiros.

1. Identificação do material bibliográfico

[X] Dissertação [ ] Tese [ ] Outro*:_____

*No caso de mestrado/doutorado profissional, indique o formato do Trabalho de Conclusão de Curso, permitido no documento de área, correspondente ao programa de pós-graduação, orientado pela legislação vigente da CAPES.

Exemplos: Estudo de caso ou Revisão sistemática ou outros formatos.

2. Nome completo do autor

Flávio Bento de Oliveira

3. Título do trabalho

Structural and electronic properties of functionalized germanene

4. Informações de acesso ao documento (este campo deve ser preenchido pelo orientador)

Concorda com a liberação total do documento [X] SIM [ ] NÃO[1]

[1] Neste caso o documento será embargado por até um ano a partir da data de defesa. Após esse período, a possível disponibilização ocorrerá apenas mediante:
a) consulta ao(à) autor(a) e ao(à) orientador(a);
b) novo Termo de Ciência e de Autorização (TECA) assinado e inserido no arquivo da tese ou dissertação.
O documento não será disponibilizado durante o período de embargo.
Casos de embargo:
- Solicitação de registro de patente;
- Submissão de artigo em revista científica;

Processo: 23070.022664/2020-53 Documento: 3394617

Obs. Este termo deverá ser assinado no SEI pelo orientador e pelo autor.

Documento assinado eletronicamente por **Flávio Bento De Oliveira**, **Discente**, em 10/12/2022, às 21:52, conforme horário oficial de Brasília, com fundamento no § 3º do art. 4º do Decreto nº 10.543, de 13 de novembro de 2020.

Documento assinado eletronicamente por **Andréia Luisa Da Rosa**, **Professor do Magistério Superior**, em 11/12/2022, às 09:40, conforme horário oficial de Brasília, com fundamento no § 3º do art. 4º do Decreto nº 10.543, de 13 de novembro de 2020.

A autenticidade deste documento pode ser conferida no site https://sei.ufg.br/sei/controlador_externo.php?acao=documento_conferir&id_orgao_acesso_externo=0 informando o código verificador **3394617** e o

Flávio Bento de Oliveira

Structural and electronic properties of functionalized germanene

Dissertação apresentada ao Programa de Pós–Graduação do Instituto de Física da Universidade Federal de Goiás, como requisito parcial para obtenção do título de Mestre em Física.

Área de pesquisa: Física da Matéria Condensada, Simulação Computacional

Orientadora: Prof. Dra. Andreia Luísa Da Rosa

Goiânia
2020

Ficha de identificação da obra elaborada pelo autor, através do
Programa de Geração Automática do Sistema de Bibliotecas da UFG.

Bento de Oliveira, Flávio
Structural and electronic properties of functionalized germanene [manuscrito] / Flávio Bento de Oliveira. - 2020.
58 f.

Orientador: Prof. Andreia Luísa Da Rosa.
Dissertação (Mestrado) - Universidade Federal de Goiás, Instituto de Física (IF), Programa de Pós-Graduação em Física, Goiânia, 2020.
Bibliografia.
Inclui siglas, gráfico, lista de figuras.

1. Germanene. 2. Functionalization. 3. First Principles Calculations. I. Luísa Da Rosa, Andreia, orient. II. Título.

CDU 53

UNIVERSIDADE FEDERAL DE GOIÁS

INSTITUTO DE FÍSICA

ATA DE DEFESA DE DISSERTAÇÃO

Ata nº 184 da sessão de Defesa de Dissertação de Flávio Bento de Oliveira, que confere o título de Mestre em Física, na área de concentração em Física.

Aos 09 dias do mês de junho de 2020, a partir das 10h00min, por meio de videoconferência, realizou-se a sessão pública de Defesa de Dissertação intitulada "Structural and electronic properties of functionalized germanene". Os trabalhos foram instalados pela Orientadora, Professora Doutora Andreia Luisa da Rosa (IF/UFG), com a participação dos demais membros da Banca Examinadora: Professora Doutora Erika Nascimento Lima (UFR), membro titular externo; e Professor Doutor Leandro Felix de Sousa Bufaiçal (IF/UFG), membro titular interno. Durante a arguição, os membros da banca não fizeram sugestão de alteração do título do trabalho. A Banca Examinadora reuniu-se em sessão secreta a fim de concluir o julgamento da Dissertação, tendo sido o candidato aprovado pelos seus membros. Proclamados os resultados pela Professora Doutora Andreia Luisa da Rosa, Presidente da Banca Examinadora, foram encerrados os trabalhos e, para constar, lavrou-se a presente ata que é assinada pelos Membros da Banca Examinadora, aos 09 dias do mês de junho de 2020.

TÍTULO SUGERIDO PELA BANCA

Documento assinado eletronicamente por **Leandro Felix De Sousa Bufaiçal**, **Professor do Magistério Superior**, em 09/06/2020, às 12:25, conforme horário oficial de Brasília, com fundamento no art. 6º, § 1º, do Decreto nº 8.539, de 8 de outubro de 2015.

Documento assinado eletronicamente por **Andréia Luisa Da Rosa**, **Professor do Magistério Superior**, em 09/06/2020, às 12:26, conforme horário oficial de Brasília, com fundamento no art. 6º, § 1º, do Decreto nº 8.539, de 8 de outubro de 2015.

Documento assinado eletronicamente por **ERIKA NASCIMENTO LIMA**, **Usuário Externo**, em 09/06/2020, às 12:28, conforme horário oficial de Brasília, com fundamento no art. 6º, § 1º, do Decreto nº 8.539, de 8 de outubro de 2015.

A autenticidade deste documento pode ser conferida no site https://sei.ufg.br/sei/controlador_externo.php?acao=documento_conferir&id_orgao_acesso_externo=0, informando o código verificador **1338186** e o código CRC **F87AF0A1**.

Agradecimentos

Gostaria de agradecer primeiramente aos meus parentes, especialmente a minha mãe, Sirlene Ribeiro de Oliveira por me incentivar nos estudos e por me dar auxilio e forças para continuar nas dificuldades encontradas na vida.

Agradeço a Prof. Dra. Andreia Luísa Da Rosa pela orientação e por me mostrar os passos para seguir uma carreira acadêmica.

Agradeço aos professores da banca pela disponibilidade.

Queria agradecer também aos professores e colegas que me apoiaram.

Por último, agradeço as instituições que fomentaram essa pesquisa como Programa de Pós-Graduação do Instituto de Física da UFG e a FAPEG.

"God does arithmetic"

– **Carl Friedrich Gauss**

Resumo

Os estudo de materiais bidimensionais (2D) tem tido interesse crescente após a descoberta do grafeno, cujas propriedades eletrônicas diferem surpreendentemente da sua forma tridimensional, o grafite. Materiais 2D têm propriedades eletrônicas, elásticas e ópticas de grande interesse para aplicações tecnológicas, bem como como um papel fundamental na redução das dimensões dos dispositivos eletrônicos que são produzidos atualmente. O grafeno é um semicondutor de gap zero, com bandas de condução e valência degeneradas nos pontos K e K', formando cones de Dirac. No entanto, dificuldades na realização e ajuste de um gap de banda no grafeno tem levado ao interesse crescente em outros materiais bidimensionais.

O germaneno, que é uma única camada de germanio, também é um semicondutor de gap zero. No entanto investigações recentes sugerem que as camadas de germânio reagem rapidamente com o ambiente. Isso pode afetar não apenas sua estrutura eletrônica, mas também sua reatividade, e suas propriedades dielétricas e ópticas. Portanto, pode-se procurar formas de modificar as propriedades dessas camadas bidimensionais. Uma rota promissora para ajustar a estrutura eletrônica de materiais em camadas é a adsorção de moléculas orgânicas ou grupos funcionais. Note-se que o germaneno foi sintetizado de forma a criar camadas híbridas mediante adsorção de ligantes orgânicos.

Neste trabalho, o ajuste do gap da banda com ligantes orgânicos adsorvidos em monocamadas bidimensionais de germânio foi investigado usando cálculos de primeiros princípios. Mostramos que a adsorção desses pequenos grupos mantém a estabilidade destas nanoestruturas de germânio. Nós propomos que a estabilidade dessas estruturas decorre não somente das deformações induzidas pela adsorção destes grupos orgânicos, mas também devido às interações ligante-ligante. Nossas descobertas abrem caminho para um *design* racional de nanoestruturas de germânio, com potencial aplicações em dispositivos eletrônicos.

Palavras - chave: Germaneno, Funcionalização, Cálculos de Primeiros Princípios

Abstract

The study of two-dimensional (2D) materials has increasing interest after the discovery of graphene whose property differed surprisingly from its three-dimensional form. 2D materials have electrical properties of great interest for technological applications, and play a role in the reduction of the dimensions of the electronic devices that are currently produced as well. Graphene in its honeycomb structure has a zero gap, with conducing and valence bands being degenerate at K and K' points, forming cones. However, difficulties in carrying out and adjusting a reasonable sizeable band gap in graphene is attracting increasing interest to other two-dimensional materials. One of the promising material is a single layer of germanium, the so-called germanene.

Recent investigations suggest that germanium layers react rapidly with the environment. This may affect not only their electronic structure, but also their reactivity and optical properties. Therefore one may search for ways of tuning the electronic properties of these two-dimensional layers. A promising route for tuning the electronic structure of bare layered materials is the adsorption of organic molecules or functional groups. Recently, germanene has been synthesized to create hybrid layers upon adsorption of organic ligands.

In this work, band gap tuning of organic ligands adsorbed on bidimensional germanium monolayers have been investigated using first-principles calculations. We show that the adsorption of these small groups retains the initially stable free-standing pristine buckled germanium nanostructures. We claim that the stability of these structures stem from both strain induced by the adsorption of this organic group and ligand-ligand interactions. Our studies of a finite band gap form the way for a rational *design* of germanium nanostructures, which can find applications in electronic devices.

Key - words: Germanene, Functionalization, First Principles Calculations

List of Figures

Summary

CHAPTER 1

Introduction

The study of two-dimensional (2D) materials has had increasing interest after the discovery of graphene whose property differed surprisingly from its three-dimensional form, graphite [1, 2]. 2D materials have electrical properties of great interest for technological applications, as well as in the reduction of the dimensions of the electronic devices that are currently produced. Graphene in its honeycomb structure has a zero gap, with conduction and valence bands being degenerate at K and K' points, forming cones. However, difficulties in carrying out and adjusting a reasonable sizeable band gap in graphene is attracting increasing interest in other two-dimensional materials, such as germanene.

Recent investigations suggest that germanium layers react rapidly with the environment [3]. This may affect not only their electronic structure, but also their reactivity and optical properties. Therefore one may search for ways of tuning the electronic properties of these two-dimensional layers. A promising route for tuning the electronic structure of bare layered materials is the adsorption of organic molecules or functional groups [4].

Indeed, germanene has been synthesized to create hybrid layers upon adsorption of organic ligands. It has been shown that modified germanium were stable hybrid materials and with tunable optical properties [3]. Although bare germanium layers have been extensively investigated, functionalized layers with organic molecules has received less attention. For example, several aspects of electronic and optical properties of organic ligand adsorbed germanium layers remain little explored.

In this work we have investigated the structural and electronic properties of germanene adsorbed with small organic groups using density-functional theory. We show that some of the adsorbed structures possess a sizeable band gap. We claim that the stability of these structures is a combined effect of both in-plane strain induced by the adsorption of organic groups and ligand-ligand interactions. Our studies of a finite band gap form the way for a rational *design* of germanium nanostructures, which can find applications in electronic devices at the nanoscale [5].

Furthermore, we also studied the electronic structure of germanene in the presence of point defects such as vacancy and larger defects such as nanopores. We show that the structures have a metallic character, which could be suitable for applications in sensing devices.

This work is divided as the following: in Chapter 2 we introduce the methodology used in this work. In Chapter 3 we present the results obtained for the functionalized germanene structures. Chapters 4 and 5 are dedicated to the results obtained for defects and pores in bare germanene. Finally, in Chapter 7 we present the conclusions for this work.

CHAPTER 2

Methodology

In a many-body system with many electrons and nuclei, the time-independent Schrödinger equation is given by:

$$\hat{\mathbf{H}}|\Psi(\{\mathbf{R}_\alpha\};\{\mathbf{r}_i\})\rangle = E|\Psi(\{\mathbf{R}_\alpha\};\{\mathbf{r}_i\})\rangle, \tag{2.0.1}$$

with $\hat{\mathbf{H}}$ being the Hamiltonian operator from the system which consists of nuclei and electrons, respectively represented by group of position vectors $\mathbf{R}_\alpha$ and $\mathbf{r}_i$. Adopting atomic units in all the equations, $\hbar = m_e = \frac{e^2}{4\pi\epsilon_0} = 1$, we have:

$$\hat{\mathbf{H}} = -\sum_{i=1}^{N}\frac{1}{2}\nabla_i^2 - \sum_{\alpha=1}^{M}\frac{1}{2M_\alpha}\nabla_\alpha^2 - \sum_{i=1}^{N}\sum_{\alpha=1}^{M}\frac{Z_\alpha}{r_{i\alpha}} + \sum_{i=1}^{N}\sum_{j>i}^{N}\frac{1}{r_{ij}} + \sum_{\alpha=1}^{M}\sum_{\beta>\alpha}^{M}\frac{Z_\alpha Z_\beta}{R_{\alpha\beta}} \tag{2.0.2}$$

The first and second terms are the kinetic energy of the electrons and nuclei, The third, fourth and fifth terms are the Coulomb interaction between nucleus and electrons, between electrons and between nuclei, respectively, where M_α is the mass and Z_α is the atomic number of the nucleus, following the notation $r_{i\alpha} = |\mathbf{r}_i - \mathbf{R}_\alpha|, r_{ij} = |\mathbf{r}_i - \mathbf{r}_j|, R_{\alpha\beta} = |\mathbf{R}_\alpha - \mathbf{R}_\beta|$.

Its impossible to calculate this system analytically, since it can only be resolved only for simple cases like hydrogen atom. Therefore approximations are needed and the problem must be solved numerically.

2.1 The Born-Oppenheimer Approximation

The Born-Oppenheimer Approximation[6] assumes that the movement of the nuclei are much slower compared to the movement of the electrons, because the mass of the nuclei is much larger than that of electron. Thus, with each nuclear movement, the electrons are arranged instantly generating a new configuration. In this way, we can

consider the nuclear movements as fixed for each electronic rearrangement step, making the kinetic part of the nuclei as a constant. Within this approximation, the second term of Eq. (2.0.2) can be neglected and the last term can be considered as a constant, decoupling the Hamiltonian operator which has the form $\hat{\mathbf{H}} = \hat{\mathbf{H}}_e + \hat{\mathbf{H}}_{Nuc}$ where $\hat{\mathbf{H}}_e$ is the electronic part and $\hat{\mathbf{H}}_{Nuc}$ is the nuclear part. Assuming that the wave functions take form:

$$\Psi(\{\mathbf{R}_\alpha\}, \{\mathbf{r}_i\}) = \psi(\{\mathbf{R}_\alpha\}, \{\mathbf{r}_i\})\phi(\{\mathbf{r}_i\}), \tag{2.1.3}$$

the Schrödinger equation involving the electronic Hamiltonian is then:

$$\hat{\mathbf{H}}_e\psi_e(\{\mathbf{R}_\alpha\}, \{\mathbf{r}_i\}) = E_e\psi_e(\{\mathbf{R}_\alpha\}, \{\mathbf{r}_i\}), \tag{2.1.4}$$

with

$$\hat{\mathbf{H}}_e = -\sum_{i=1}^{N}\frac{1}{2}\nabla_i^2 - \sum_{i=1}^{N}\sum_{\alpha=1}^{M}\frac{Z_\alpha}{r_{i\alpha}} + \sum_{i=1}^{N}\sum_{j>i}^{N}\frac{1}{r_{ij}}. \tag{2.1.5}$$

The electronic wave function ($\psi_e(\{\mathbf{R}_\alpha\}, \{\mathbf{r}_i\})$) explicitly depends on the coordinates of the electrons and parametrically on the nuclei coordinates. The total energy E_{tot} of the system is then written as:

$$E_{tot} = E_{ele} + \sum_{\alpha=1}^{M}\sum_{\beta>\alpha}^{M}\frac{Z_\alpha Z_\beta}{R_{\alpha\beta}} \tag{2.1.6}$$

The second term in Eq.2.1.6 deals with the repulsive forces of nuclei, which is constant, due to the decoupling of the nuclear and electronic movements.We were able to reduce a N_e electron and N_{Nuc} nuclei problem to just a N_e electrons problem. However the electronic problem remains without analytical solution for most cases. In this work this problem is solved using Density Functional Theory(DFT)[7], described below.

2.2 Density Functional Theory(DFT)

The Density Functional Theory (DFT) initially proposed by Hohenberg and Kohn [7], consists of two theorems, which are based on the works of Thomas and Fermi in the 1920s [8, 9]. Hohenberg and Kohn (HK) considered as variable the electronic density, with density becoming a functional of the electronic wave function,

By doing so, the density of the state of an electronic system is:

$$n(\mathbf{r}) = \int \dots \int \psi^*(\mathbf{r}_1, \mathbf{r}_2, \dots \mathbf{r}_N)\psi(\mathbf{r}_1, \mathbf{r}_2, \dots \mathbf{r}_N)d\mathbf{r}_N \tag{2.2.7}$$

where $\psi(\mathbf{r}_1, \mathbf{r}_2, \dots \mathbf{r}_N)$ is the ground state wave function. The two theorems of Hohenberg and Kohn are enunciated below.

2.2.1 The first Hohenberg-Kohn theorem

The first theorem states:
The density of the ground state of an electronic system $n_0(\boldsymbol{r})$ within a trivial additive constant, is uniquely characterized by the external potential $v_{ext}(\boldsymbol{r})$.
With the electronic density of the system one can determine the external potential and the number of electrons and the Hamiltonian of the system, the total energy functional $E_v[n]$ is described as

$$E_v[n] = \int n(\mathbf{r})v(\mathbf{r})d\mathbf{r} + F_{HK}[n] \tag{2.2.8}$$

where

$$F_{HK}[n] = T[n] + E_{ee}[n] \tag{2.2.9}$$

Where $T[n]$ and $E_{ee}[n]$ are kinetic energy and energy due to the electron-electron interaction, respectively. To prove the first theorem, one should make a **reductio ad absurdum**.

Assuming that there are two distinct external potentials, v_1 and v_2, with $\hat{\mathbf{H}}^{(1)}$ and $\hat{\mathbf{H}}^{(2)}$ respectively, both same density $n(\mathbf{r})$, for v_1 we have $E_0^1 < \langle\psi^{(2)}|\boldsymbol{H_1}|\psi^{(2)}\rangle$ where E_0^1 and E_0^2 are groundstates.

$$\langle\psi^{(2)}|\boldsymbol{H_1}|\psi^{(2)}\rangle = \langle\psi^{(2)}|\boldsymbol{H_2}|\psi^{(2)}\rangle + \langle\psi^{(2)}|\boldsymbol{H_1} - \boldsymbol{H_2}|\psi^{(2)}\rangle \tag{2.2.10}$$

$$\langle\psi^{(2)}|\boldsymbol{H_1}|\psi^{(2)}\rangle = E_0^2 + \langle\psi^{(2)}|\boldsymbol{H_1} - \boldsymbol{H_2}|\psi^{(2)}\rangle \tag{2.2.11}$$

Using the (Eq.2.2.9) on 2.2.10, we have

$$E_0^1 < E_0^2 + \int n(\mathbf{r})[v_1(r) - v_2(r)]dr \tag{2.2.12}$$

repeat the same for E_0^2

$$E_0^2 < E_0^1 + \int n(\mathbf{r})[v_2(r) - v_1(r)]dr \tag{2.2.13}$$

sum the equations (2.2.13) and (2.2.14), which results in:

$$E_0^{(1)} + E_0^{(2)} < E_0^{(1)} + E_0^{(2)} \tag{2.2.14}$$

Thus, we can conclude that two distinct external potentials do not lead to the same density, and by absurd $\square$.

2.2.2 The second Hohenberg-Kohn theorem

The second theorem is:
The energy of the ground state corresponds to the minimum of the functional $E_0[n_0(\boldsymbol{r})]$*, any different density* $n(\boldsymbol{r}) \neq n_0(\boldsymbol{r})$ *will result in* $E[n(\boldsymbol{r})] > E_0[n_0(\boldsymbol{r})]$.

The second Hohenberg-Kohn theorem provides the variational principle. For a trial electron density $n(\mathbf{r}) \geq 0$ and $\int n(\mathbf{r})d\mathbf{r} = N_e$, then

$$E_v[n] = \int v(\mathbf{r})n(\mathbf{r})d\mathbf{r} + F_{HK}[n] \geq E_v[n_0] \tag{2.2.15}$$

Assuming differentiation of $E_v[n]$, the variational principle requires that the ground-state density satisfies the stationary principle. Using the Lagrange multiplier method, we have:

$$\delta\left\{ E_v[n] - \mu\left[\int n(\mathbf{r})d\mathbf{r} - N_e\right]\right\} = 0 \tag{2.2.16}$$

where μ is the lagrange multiplier and physically our chemical potential. This gives the Euler-Lagrange equation:

$$\mu = \frac{\delta E_v[n]}{\delta n(\mathbf{r})} = v(\mathbf{r}) + \frac{\delta F_{HK}[n]}{\delta n(\mathbf{r})} \tag{2.2.17}$$

Therefore, this is the exact functional called HK (F_{HK}) that describes precisely my problem of many bodies, however, the exact form of this functional is not known, so aproximations are required to resolve the desired system. A proposed solution done by Kohn and Sham [10] using aproximations will be described on the next session

2.2.3 The Kohn-Sham equations

We have seen in the past section that the ground state energy for many electron system is:

$$E_v[n] = \int v(\mathbf{r})n(\mathbf{r})d\mathbf{r} + F_{HK}[n] \tag{2.2.18}$$

Kohn and Sham proposed a scheme which allow to simplify the application of the DFT. They proposed that the kinetic energy and potential are separated into components, two component being the energy of non-interacting electrons $T_s[n]$ and the others components is included in the exchange and correlation function $E_{xc}[n]$, thus writing the equation as:

$$F_{HK}[n] = J[n] + T_s[n] + E_{xc}[n], \tag{2.2.19}$$

where the first term is the classical electrostatic repulsion (Hartree term). We then have:

$$J[n] = \frac{1}{2}\iint \frac{n(\mathbf{r})n(\mathbf{r}')}{|\mathbf{r}-\mathbf{r}'|}d\mathbf{r}d\mathbf{r}' \qquad ; \qquad T_s[n] = -\frac{1}{2}\sum_i \int \phi_i^*(\mathbf{r})\nabla^2\phi_i(\mathbf{r})d\mathbf{r} \tag{2.2.20}$$

where $\phi_i(\mathbf{r})$ are Kohn-Sham orbitals. According to the Kohn-Sham formalism, the Kohn-Sham orbitals should be orthonormal:

$$\int \phi_i^*(\mathbf{r})\phi_j(\mathbf{r})d(\mathbf{r}) = \delta_{ij}. \tag{2.2.21}$$

The total energy then takes the form:

$$E_v[n] = \frac{1}{2}\iint \frac{n(\mathbf{r})n(\mathbf{r}')}{|\mathbf{r}-\mathbf{r}'|}d\mathbf{r}d\mathbf{r}' - \frac{1}{2}\sum_i \int \phi_i^*(\mathbf{r})\nabla^2\phi_i(\mathbf{r})d\mathbf{r} + E_{xc}[n] + \int n(\mathbf{r})v(\mathbf{r})d\mathbf{r}. \tag{2.2.22}$$

Using the Lagrange multipliers in the Eq.(2.2.22), the second theorem HK leads to:

$$\int \delta n(\mathbf{r})\left[v(\mathbf{r}) + \frac{\delta T_s[n]}{\delta n} + \int \frac{n'(\mathbf{r}')}{|\mathbf{r}-\mathbf{r}'|} + \frac{\delta E_{xc}[n]}{\delta n} - \epsilon\right]d\mathbf{r} = 0 \tag{2.2.23}$$

$$V_{\text{eff}}(\mathbf{r}) = v(\mathbf{r}) + \int \frac{n'(\mathbf{r}')}{|\mathbf{r}-\mathbf{r}'|} + v_{xc}[n] \tag{2.2.24}$$

where $v_{xc}[n]$ is the exchange-correlation potential:

$$\frac{\delta E_{xc}[n]}{\delta n} = v_{xc}[n]. \tag{2.2.25}$$

We obtain the following equation:

$$\frac{\delta T_s[n]}{\delta n} + V_{\text{eff}}(\mathbf{r}) = \mu \tag{2.2.26}$$

These equations were obtained for a non-interacting electron system in the presence of an external potential. With this we obtain the Kohn-Sham Hamiltonian

$$\hat{\mathbf{H}}^{KS} = -\frac{1}{2}\nabla^2 + V_{eff}(\mathbf{r}). \tag{2.2.27}$$

$$\hat{\mathbf{H}}^{KS}\phi_i(\mathbf{r}) = E_e\phi_i(\mathbf{r}) \tag{2.2.28}$$

and define density as

$$n(\mathbf{r}) = \sum_i |\phi_i(\mathbf{r})|^2. \tag{2.2.29}$$

The Eqs.(2.2.24), (2.2.28) and (2.2.29) are the so-called Kohn-Sham equations. These equations are solved self-consistently, as shown below.

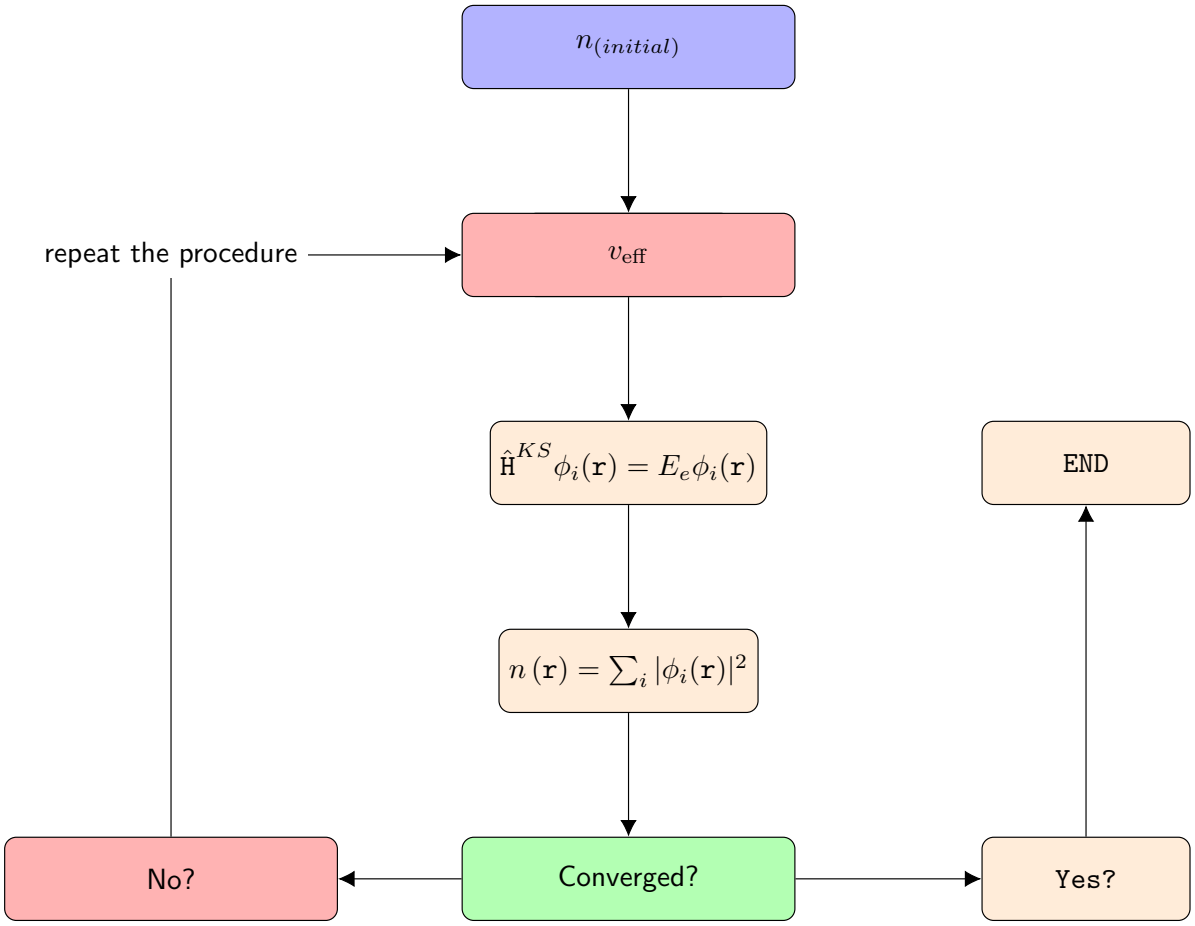

Figure 2.1. Typical fluxogram for a self-consistent calculation using Kohn-sham equations.

It follows then, that the total energy is calculated as:

$$E_e[n] = \int n(\mathbf{r})v(\mathbf{r})d\mathbf{r} + T[n] + E_{xc}[n] + \frac{1}{2}\iint \frac{n(\mathbf{r})n(\mathbf{r}')}{|r-r'|}d\mathbf{r}d\mathbf{r}' \tag{2.2.30}$$

Isolating the potential in Eq. (2.2.24) and substituting in Eq. (2.2.31), we have

$$\begin{aligned} E_e[n] &= T[n] + \int v_{\text{eff}}(\mathbf{r})n(\mathbf{r})d(\mathbf{r}) - \iint \frac{n(\mathbf{r})n(\mathbf{r}')}{|r-r'|}d\mathbf{r}d\mathbf{r}' \\ &\quad - \int v_{xc}(\mathbf{r})n(\mathbf{r})d(\mathbf{r}) + \frac{1}{2}\iint \frac{n(\mathbf{r})n(\mathbf{r}')}{|r-r'|}d\mathbf{r}d\mathbf{r}' + E_{xc}[n] \end{aligned} \tag{2.2.31}$$

called $\sum_i \epsilon_i = T[n] + \int v_{\text{eff}}(\mathbf{r}) n(\mathbf{r}) d(\mathbf{r})$, we have

$$E_e[n] = \sum_i \epsilon_i - \frac{1}{2} \iint \frac{n(\mathbf{r}) n(\mathbf{r}')}{|r - r'|} d\mathbf{r} d\mathbf{r}' + E_{xc}[n] - \int v_{xc}(\mathbf{r}) n(\mathbf{r}) d(\mathbf{r}) \tag{2.2.32}$$

We then reduce the many-body problem of nuclei and electrons to several one electron problems. The exact form of the exchange-correlation potential is unfortunately unknown and need to be approximated[10]. In the next section we will show some approximations for the exchange-correlation potential.

2.2.4 Local Density Approximation

The first exchange-correlation approach to the Kohn-Sham equations is the Local Density Approximation (LDA). It assumed that the electronic density$[n]$ is equal to that of a homogeneous electron gas. The exchange-correlation energy in the local-density approximation is given by

$$E_{xc}^{LDA}[n] = \int n(\mathbf{r}) \epsilon_{xc}^{hom} n(\mathbf{r}) d\mathbf{r}, \tag{2.2.33}$$

where ϵ_{xc}^{hom} is the exchange-correlation energy of a homogeneous electron gas, using Eq.(2.2.25), we have

$$v_{xc}^{LDA} = \epsilon_{xc}^{hom}(n(\mathbf{r})) + \frac{n(\mathbf{r}) \partial \epsilon_{xc}^{hom}}{\partial n(\mathbf{r})}. \tag{2.2.34}$$

The Kohn-Sham equations using potential LDA, takes the form

$$\left[-\frac{1}{2} \nabla^2 + v(\mathbf{r}) + \int \frac{n(\mathbf{r'})}{|\mathbf{r} - \mathbf{r'}|} d\mathbf{r} + v_{xc}^{LDA}(n(\mathbf{r}) \right] \psi_i = \epsilon_i \psi_i. \tag{2.2.35}$$

The functional ϵ_{xc}^{hom} can be written as

$$\epsilon_{xc}^{hom} = \epsilon_x^{hom} + \epsilon_c^{hom} \tag{2.2.36}$$

where ϵ_x^{hom} is the energy of a homogeneous gas, given as:

$$\epsilon_x^{hom}(n(\mathbf{r})) = -\left(\frac{3}{4}\right)\left(\frac{3}{\pi}\right)^{1/3} n(\mathbf{r})^{1/3} \tag{2.2.37}$$

ϵ_c^{hom} even for a homogeneous electron gas can not be determined exactly. Cerpeley and Alder[11] using quantum Monte Carlo simulation for an interacting homogeneous electron gas, the paper has shown good results, for that these energies are parameterized, so that the electronic density is uniform. More recently Perdew and Zunger[12] also parameterized the LDA exchange-correlation potential:

$$\epsilon_c^{hom} = -0.1423\,(1 + 1.0529\sqrt{r_s} + 0.3334 r_s)^{-1} \quad \text{if} \quad r_s \geq 1 \tag{2.2.38}$$

$$= -0.0480 + 0.0311 ln r_s - 0.0116 r_s + 0.002 r_s ln r_s \quad \text{if} \quad 0 \leq r_s \ll 1, \tag{2.2.39}$$

where $r_s = (4\pi(\mathbf{r}/3)^{-1/3}$ is the so-called Wigner-Seitz radius.

Local Density Approximation was the main approximation used for functional exchange-correlation for several years. However LDA is not a good approximation for non-uniform electron densities, with difficulties in calculating the band widths in the semiconductor band structure[13, 14]. This lead to new approximations, such as the Generalized Gradient Approximation (GGA), as described next.

2.2.5 The Generalized Gradient Approximation

In the Generalized Gradient Approximation(GGA), the functional E_{xc} depend on the local-density $n(\mathbf{r})$ and on the gradient of the total charge density $|\nabla n(\mathbf{r})|$:

$$E_{xc}^{GGA}[n] = \int F_{xc}\,[n(\mathbf{r}), |\nabla n(\mathbf{r})|]\, d\mathbf{r} \tag{2.2.40}$$

The Eq.(2.2.40) must be parameterized. There are several proposed schemes, as described in Refs.[15, 16, 17]. In this work will use the Perdew, Burke and Ernzerhof or PBE[17]. In the GGA-PBE, the parameterization of the factor F_{xc} is given by:

$$E_{xc}^{GGA}[n] = \int n(\mathbf{r}) \epsilon_{xc} F_{xc}\,[r_s, s]\, d\mathbf{r} \tag{2.2.41}$$

where r_s is the local Seitz radius ($n = \frac{3\pi r_s^3}{4}$) and $s(\mathbf{r}) = \frac{|\nabla n|}{2 k_F n}$ is a dimensionless density gradient. The exchange E_x is:

$$E_x^{PBE} = \int d\mathbf{r} n \epsilon_x F_x(s) \tag{2.2.42}$$

with $\epsilon_x = \frac{-3e^2 k_F}{4\pi}$.

The functional takes the form:

$$F_x^{PBE}(s) = 1 + \kappa - \frac{\kappa}{1 + \frac{\mu s^2}{\kappa}} \tag{2.2.43}$$

with $\kappa = 0.8004$. For the correlation part:

$$E_c^{GGA} = \int d\mathbf{r} n \left[\epsilon_c(rs) + H_c^{PBE}(r_s, t)\right], \tag{2.2.44}$$

with

$$H_c^{PBE}(r_s,t) = \frac{1-ln2}{\pi^2} ln\left[1 + \frac{\beta t^2}{\frac{1-ln2}{\pi^2}}\left(\frac{1+At^2}{1+At^2+A^2t^4}\right)\right], \tag{2.2.45}$$

$$A = \frac{\beta}{\gamma}\left[e^{-\epsilon_c^{unif}} - 1\right]^{-1} \tag{2.2.46}$$

where $t = \frac{|\nabla n|}{2k_s n}$ is a dimensionless density gradient and $\beta \simeq 0.066725$. However the functionals GGA in some cases underestimate the bandgap and band widths. Therefore, is current state of the art to use more modern functionals, such as the hybrid functionals, as described below.

2.2.6 Hybrid functionals

The hybrid functionals are functionals which add some amount of Hartree–Fock exchange energy to other functionals. The first work on hybrid functionals was by Axel Becke *et al* in 1993 [18]. Other hybrid functional include the works of Refs. [19, 20, 21]. To exemplify we cite the HSE (Heyd–Scuseria–Ernzerhof) [22] (HSE06) functionsl, where the E_{xc}^{HSE} is given by:

$$E_{xc}^{HSE} = \frac{1}{4}E_xHF + \frac{3}{4}E_x^{PBE,SR} + E_x^{PBE,LR} + E_c^{PBE}. \tag{2.2.47}$$

The terms $E_x^{PBE,SR}$ and $E_x^{PBE,LR}$ are the short-range (SR) and long-range (LR) components of the PBE exchange functional, respectively. E_c^{PBE} is the energy correlation from PBE functional and E_xHF is given by:

$$E_x^{HF} = -\frac{e}{2}\sum f_{nk}f_{mk} \times \int\int d\mathbf{r}d\mathbf{r}'\mathbf{r}ac\psi_{nk}^*(\mathbf{r})\psi_{mq}^*(\mathbf{r}')\psi_{nk}^*(\mathbf{r}')\psi_{mq}^*(\mathbf{r})|\ \mathbf{r}-\mathbf{r}\ |, \tag{2.2.48}$$

where the q and k are contained in the first Brillouin zone and the wave $\psi_{nk}^*(\mathbf{r}')$ one electron Bloch states.

2.3 The Projector augmented wave method (PAW)

The pseudo potentials approach is used to reduce the complexity of the many body electronic problem. Pseudopotentials allow simple derivation of the Kohn-Sham equations. The idea in this method is to eliminate the electrons close to the nuclei by treating them as inert (frozen core approximation). This is a good approximation if we are interested in system properties that depend on the valence electrons only. The main objective is to eliminate the nodes of the core functions so that potentials become soft.

The use of norm-conserved pseudopotentials in ab initio methods were described firstly in Refs. [23, 24, 25]. These pseudopotentials are generated from calculations of the atomic orbitals of all system, which satisfy a couple of conditions.

i. The valence pseudofunctions should not have nodes, i.e. the pseudofunction should be soft

ii. For the each valence orbital with angular momentum l, there is a cutoff radius r_c for which the radial pseudofunction(PS) (R^{ps}) should be equal to the normalized radial all-electron(AE) wave function(R^{AE});

$$R^{ps}(r) = R^{AE}(r) \qquad r > r_c \tag{2.3.49}$$

This condition allows the choice of the core region and the valence region, controlling the number of plane waves to describe the system.

iii. Similar to the above condition, the total charge should be equal, i.e.

$$\int_0^{r_c} |R^{ps}(r)|^2 dr = \int_0^{r_c} |R^{AE}(r)|^2 dr \tag{2.3.50}$$

iv. The all-electron and pseudopotential eigenvalues must be equal

$$\epsilon^{ps} = \epsilon^{AE} \tag{2.3.51}$$

v. The logarithmic derivative of the wave function of all electrons and the function of the pseudopotential must be equal and the first derivative of the energy as well.

Similarly to the pseudopotential, we use the projector augmented wave method (PAW), which allow calculations to be performed with greater computational efficiency, as described in Refs. [26, 27, 28].

Consider a pseudofunction $|\tilde{\psi}\rangle$ and the all-electron wavefunction $|\psi\rangle$.There is a linear transformation $\boldsymbol{\tau}$, where the pseudofunction is orthogonal and is exactly equal to all-electron function in the region ($r > r_c$). We have then:

$$|\psi\rangle = \boldsymbol{\tau}|\tilde{\psi}\rangle = \sum_n c_n |\psi_n\rangle. \tag{2.3.52}$$

Expanding the pseudopotential in partial waves up to n-th:

$$|\tilde{\psi}\rangle = \sum_n c_n |\tilde{\psi}_n\rangle \tag{2.3.53}$$

so we have

$$|\psi\rangle = |\tilde{\psi}\rangle + \sum_n c_n \left[|\psi_n\rangle - |\tilde{\psi}\rangle\right] \tag{2.3.54}$$

with the operator$\boldsymbol{\tau}$ being linear. We can then calculate the coefficients:

$$c_n = \langle \tilde{p_n}|\tilde{\psi}\rangle \tag{2.3.55}$$

where $\langle \tilde{p_n}|$ are projector functions, there is exactly one projector function for each partial wave. The method needs to be so that $\langle \tilde{p_n}|\tilde{\psi_m}\rangle = \delta_{nm}$ and that expanding to the center $\sum_n |\tilde{\psi_m}\rangle\langle \tilde{p_n}|\tilde{\psi}\rangle$ of pseudo functions is equal to it so obtaining the linear transformation

$$\boldsymbol{\tau} = \mathbf{1} + \sum_n \left[|\psi_n\rangle - |\tilde{\psi_n}\rangle\right] \langle \tilde{p_n}|. \tag{2.3.56}$$

As we are dealing with it pseudopotentials, in the previous session we said that the nucleus electrons are inert. The transformation $\boldsymbol{\tau}$ produces only wave functions orthogonal to the core electrons. Applying to a given operator B, with the transformation $\tilde{\mathbf{B}} = \boldsymbol{\tau}'\mathbf{B}\boldsymbol{\tau}$, so that it smooths the all-electron wave function.

$$\tilde{\mathbf{B}} = \mathbf{B} + \sum_{nm} |\tilde{p_n}\rangle \left[\langle\psi_n|\mathbf{B}|\psi_m\rangle - \tilde{\psi_n}|\mathbf{B}|\tilde{\psi_m}\rangle\right] \langle \tilde{p_m}| \tag{2.3.57}$$

Coulomb interactions, kinetic energy, etc. can be then replaced by soft functions.

2.4 Periodic systems and plane waves

Consider that the atoms are in the positions $\mathbf{R}_i$ with $\mathbf{R}_i = n_1\mathbf{a}_1 + n_2\mathbf{a}_2 + n_3\mathbf{a}_3$, where $\mathbf{a}_1, \mathbf{a}_3, \mathbf{a}_3$ are the primitive lattice vectors of the supercell in the real space and n_1, n_2, n_3 are integers. A periodic system must obey the Bloch theorem, so we can write:

$$\psi_{i\mathbf{k}(\mathbf{r})} = e^{i\mathbf{k}\cdot\mathbf{r}} u_{i\mathbf{k}}(\mathbf{r}) \tag{2.4.58}$$

where i is the band index, $\mathbf{k}$ is a point in the first Brillouin zone(BZ) and $u_{i\mathbf{k}(\mathbf{r})}$ is a periodic function in real space lattice, i.e.

$$u_{i\mathbf{k}}(\mathbf{r} + \mathbf{R}_i) = u_{i\mathbf{k}}(\mathbf{r}). \tag{2.4.59}$$

Expanding into Fourier the Eq.(2.4.59)

$$u_{i\mathbf{k}}(\mathbf{r}) = \frac{1}{\sqrt{V}} \sum_{\mathbf{G}} C_{i,\mathbf{k}+\mathbf{G}} e^{i\mathbf{G'}\cdot\mathbf{r}}, \tag{2.4.60}$$

where V is the volume of the cell and **G'** is a vector of the reciprocal lattice ,thus we can calculate the function

$$\psi_{i\mathbf{k}(\mathbf{r})} = \frac{1}{\sqrt{V}} \sum_{\mathbf{G}} C_{i,\mathbf{k}+\mathbf{G}} e^{i(\mathbf{k}+\mathbf{G})\cdot\mathbf{r}}. \tag{2.4.61}$$

We can write Eq. (2.2.27) then as

$$\sum_{\mathbf{G}} \left[\frac{1}{2}|\mathbf{k}+\mathbf{G}|^2 \delta_{\mathbf{G}\mathbf{G}'} + v\left(\mathbf{G}-\mathbf{G}'\right) + v_{\mathbf{H}}\left(\mathbf{k}-\mathbf{G}'\right) + v_{xc}\left(\mathbf{k}-\mathbf{G}'\right) \right] C_{i,\mathbf{k}+\mathbf{G}'} = \epsilon_{i\mathbf{k}} C_{i,\mathbf{k}+\mathbf{G}}. \tag{2.4.62}$$

as we are dealing with a periodic system, $|\mathbf{k}+\mathbf{G}|$ must have a limit. The expansion in plane-waves includes terms with a certain cutoff:

$$E_{\text{cut}} \leq \frac{1}{2}|\mathbf{k}+\mathbf{G}|^2. \tag{2.4.63}$$

2.5 Computational details

In this work, we compute the electronic and structural properties using the VASP (Vienna Ab-initio Simulation Package) computational code [29, 26]. The calculations presented here have been perfomrmed with $E_{\text{cut}} = 300$ eV according to the convergence test as shown in the following chapter. We use the PAW [27] method together with the exchange-correlation functional in the PBE parametrization [17]. The criteria used for the energy convergence was 10^{-4} eV.

CHAPTER 3

Bare and ligand modified germanene

3.1 Convergence tests

Before starting all calculations, we did several convergence tests to determine the optimum parameters to perform further calculations. For the generation of k-points, we did convergence tests for several meshes, starting from a $(8 \times 8 \times 1)$ mesh up to a $(12 \times 12 \times 1)$ mesh, which we use for all calculations in this work. Also convergence tests for energy cutoff shown in 3.1 leads to a conclusion that 300 eV is enough to describe the formation energies and therefore suitable to perform all further calculations.

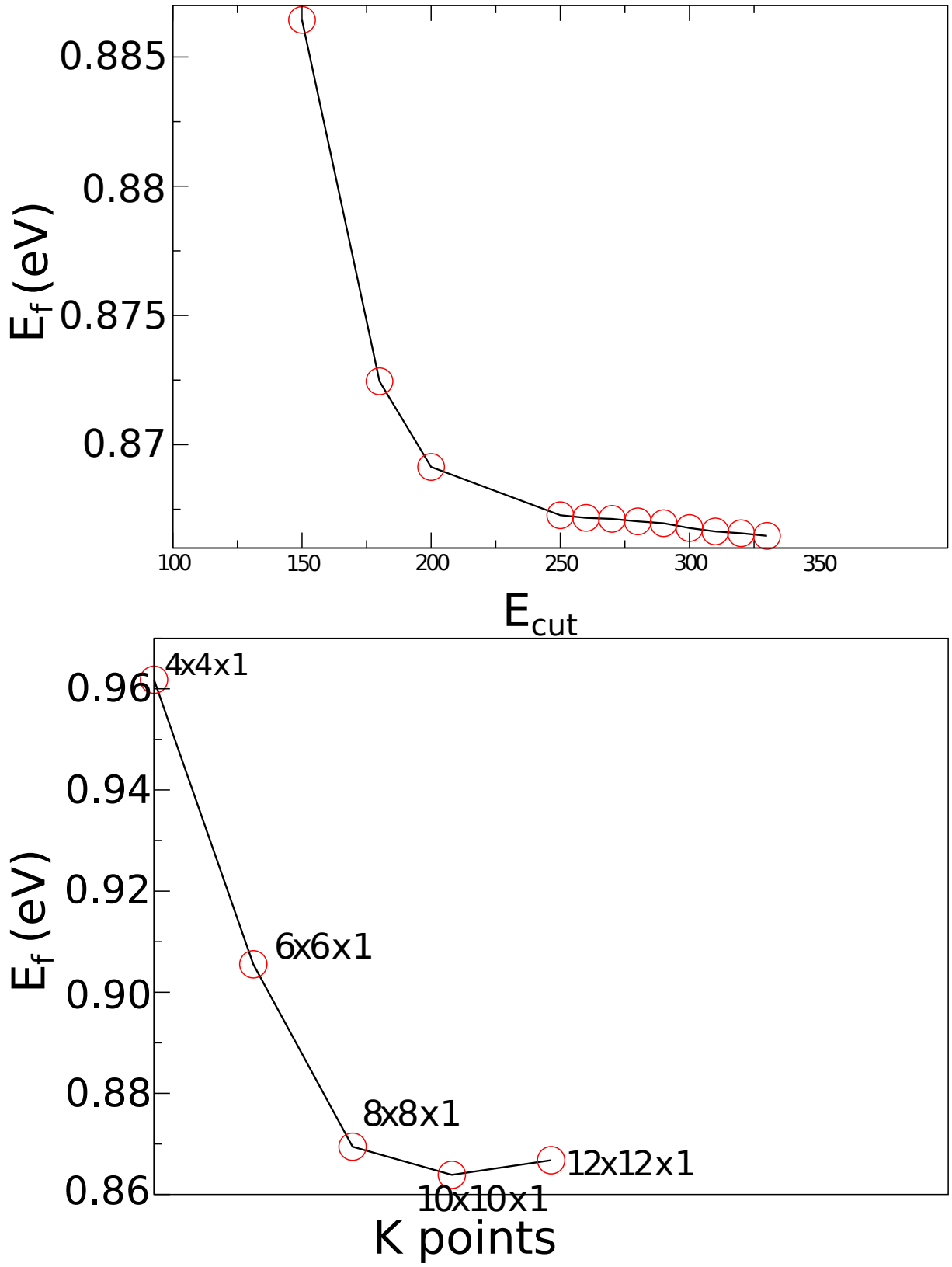

Figure 3.1. Upper panel: Formation energy of germanene as a function of energy cutoff E_{cut}. Lower panel: Formation energy of germanene as a function of k-point mesh.

3.2 Bare germanene

Bulk germanium has a fcc (face-centered cubic) lattice with 2 atoms in the unit cell forming a diamond structure, as shown in Fig. 3.2. The optimized lattice parameter is $a = 5.65$ Å, in good agreement with Ref. [30].

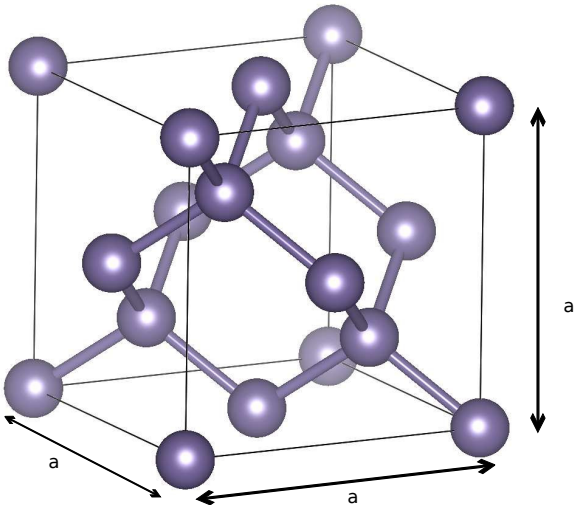

Figure 3.2. Atomic geometry of bulk germanium in the diamond structure.

We optimized the bulk germanium in order to calculate the most stable structure. Once we have done that, we construct a single layer of germanium, along the [111] direction as shown in Fig. 3.3(a). The Grey spheres represent the germanium upper plane and the yellow spheres represent germanium lower plane, as shown in Fig. 3.3(b).

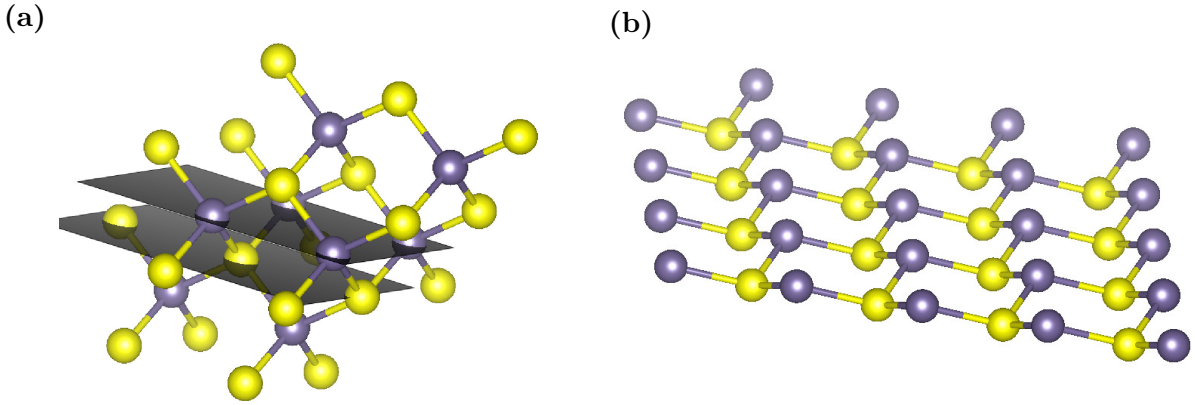

Figure 3.3. (a)Ge(111) plane and (b) single layer germanium (germanene).

Experimentally, germanene has been synthesized by dry deposition of germanium onto Au (111) surface by Dávila *et al* [31]. In these experiments the corrugated germanene on Au substrate has a buckling range of 0.41-1.50 Å. Another possible configuration of germanene is the planar one, as shown in Fig. 3.4(a).

In order to determine the stability of the atomic structure of germanene we have calculate the atomic structure of single layer germanium in both planar and corrugated

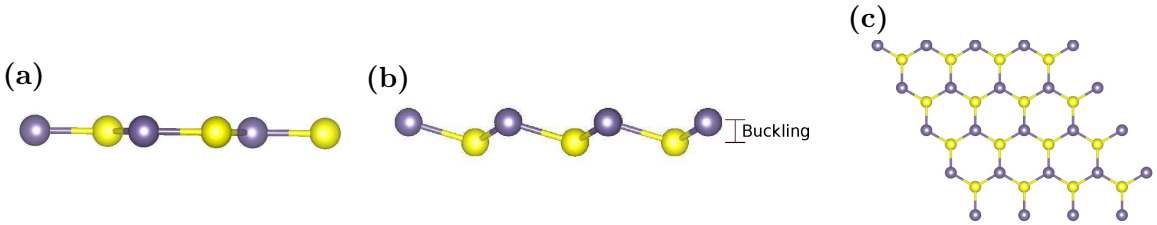

Figure 3.4. Relaxed structures of single-layer germanene. (a) planar germanene (side-view), (b) corrugated germanene (side-view) and (c) top view of both planar and corrugated germanene. Blue and yellow spheres are germanium atoms.

configurations. All calculations included spin-orbit coupling. We vary the in-plane lattice parameter $\mathbf{a} = \mathbf{b}$. For the planar structure the lattice parameter of the most stable structure was 4.12 Å and the Ge-Ge distance was 2.37 Å. The calculated lattice parameter for the ground state of corrugated germanene was 4.05 Å with a buckling of 0.69 Å and Ge-Ge distance of 2.43 Å.

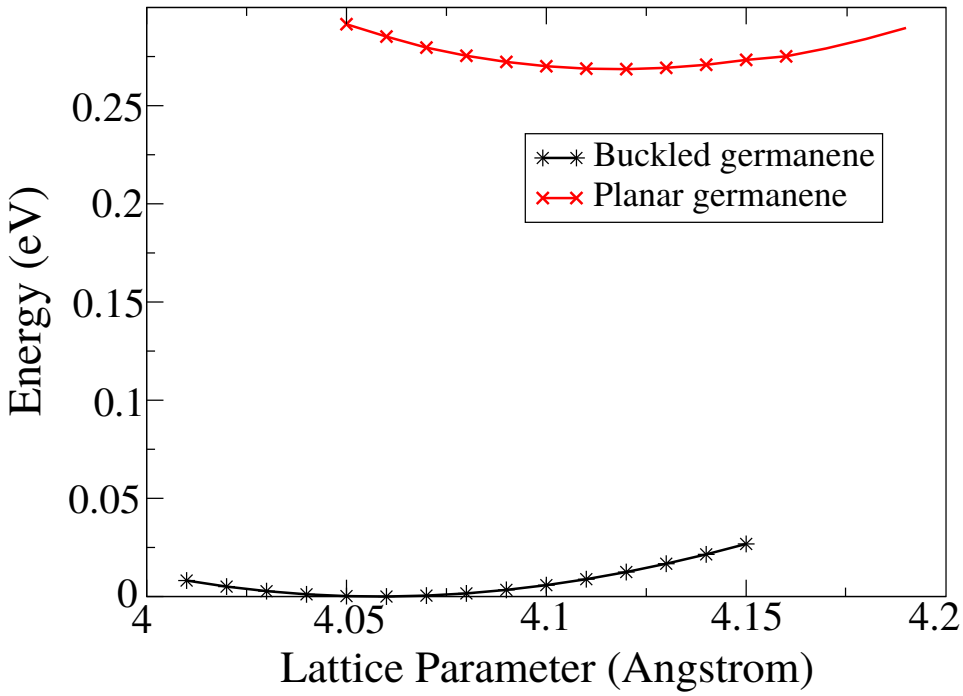

Figure 3.5. Energy as a function of the lattice parameter for corrugated and planar germanene. The zero of energy zero is set to the lowest energy found for corrugated germanene.

The results for the stability of germanene is shown in Fig. 3.5. Our results indicate that the corrugated germanene is energetically more stable than the planar germanene. The energy difference is 0.25 eV/cell.

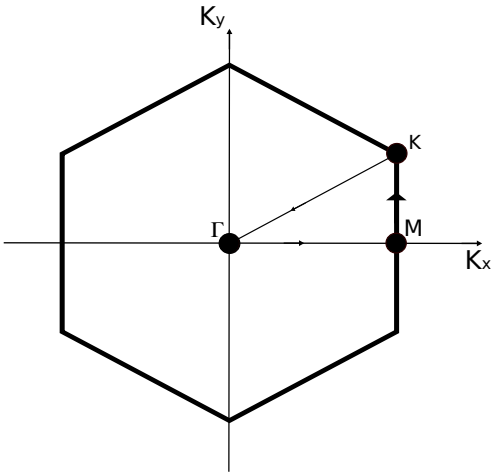

Figure 3.6. First Brillouin Zone of germanene with symmetry lines.

Now using the optimized lattice parameter, we are able to calculate the band structure of the corrugated germanene including spin-orbit coupling. In Fig. 3.6 the first Brillouin Zone of germanene with high symmetry lines is shown. We choose the path along the $\Gamma - \mathbf{M} - \mathbf{K} - \Gamma$ high symmetry lines.

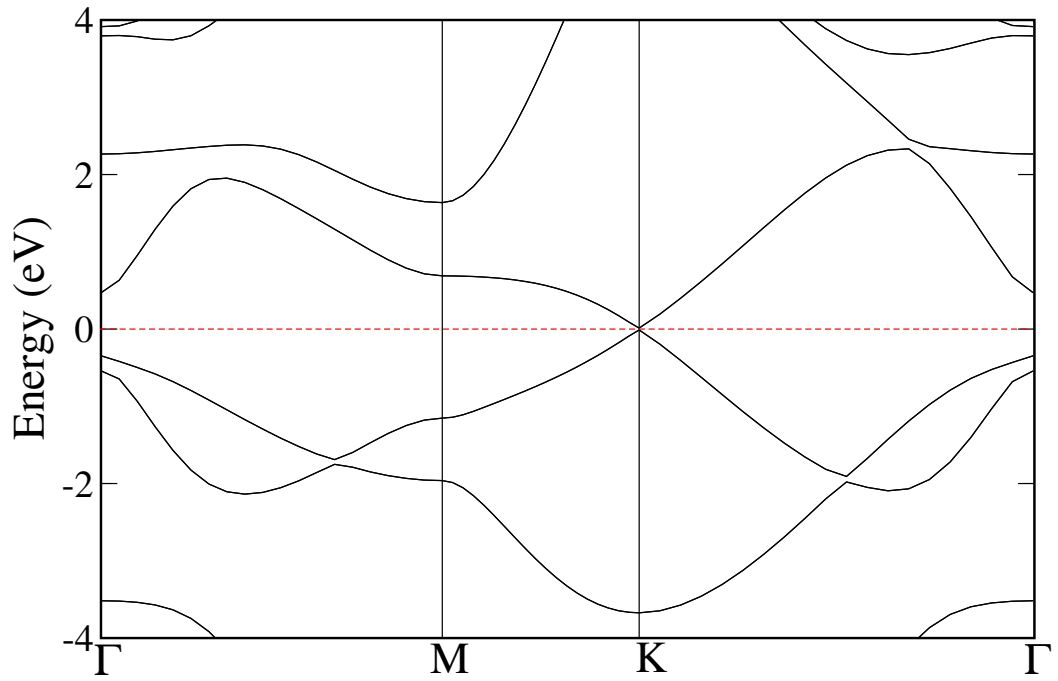

Figure 3.7. Band structure of bare germanene where dashed line is the Fermi energy.

In Fig. (3.7) we can see that the valence and conduction bands form a Dirac cone close to the Fermi energy. This direct gap is due to spin-orbit coupling, there was a symmetry break at the K point. Similar results have been found for silicene in Ref. [32]. However this feature does not exist in graphene [33], although graphene shares the same valence and conduction bands features.

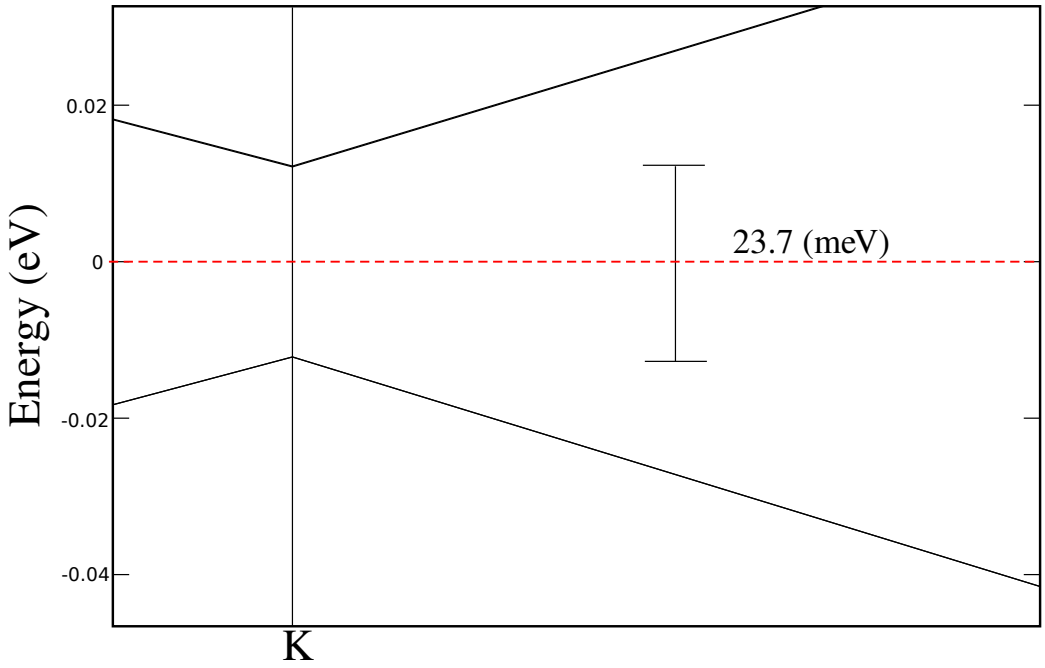

Figure 3.8. Zoom near the K point for the band structure of bare germanene. The Fermi level is set at zero.

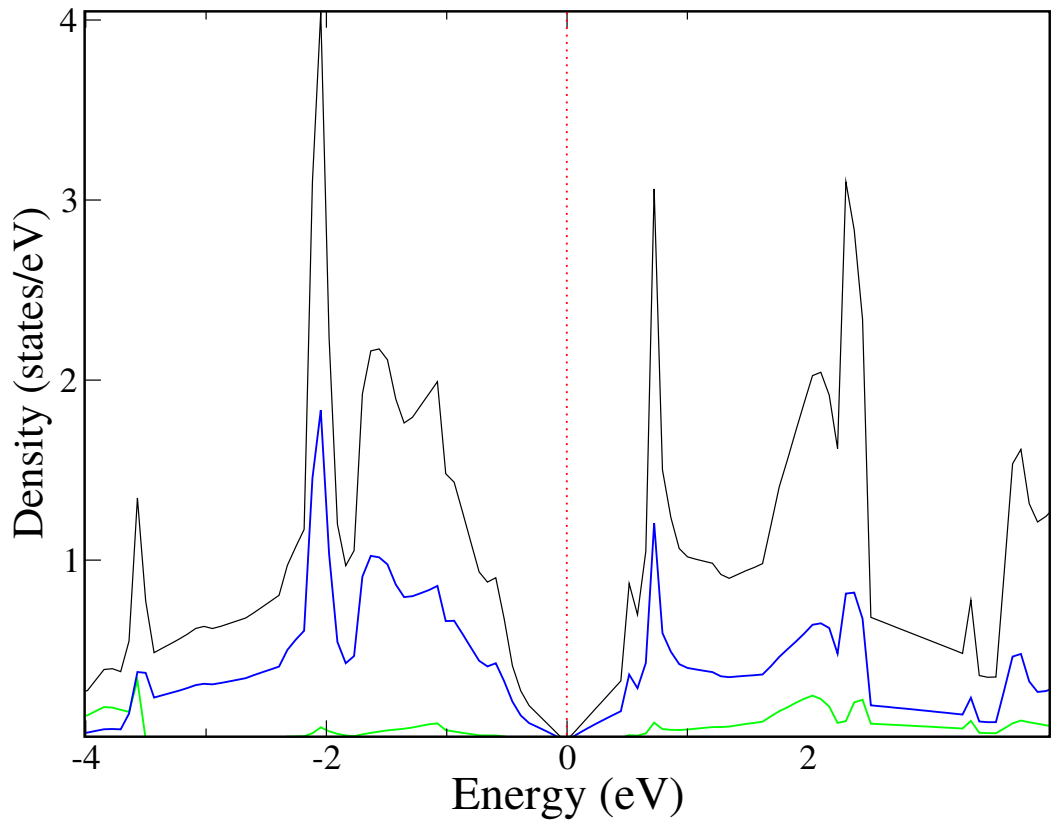

Figure 3.9. Density of states of bare germanene. The Fermi level is set at zero.

In Fig. (3.8) we see that a tiny band gap of $E_g = 23$ meV at K point exists. This result is in very good agreement with the ones in Refs. [34, 35, 32]. We have also calculated the density of states of germanene, as shown in Fig.(3.9). Large contributions of p orbitals in the valence and conduction bands are seen. In particular, the p_z orbital, as expected.

3.3 Modification of germanene with organic ligands

As we can see from the results discussed above, single layer germanene behaves as a metal. However, in order to be suitable for optoelectronic devices, there is a need of opening a sizeable band gap in these layers. There are several strategies for doing that, including doping, strain and surface and edge functionalization. In this work we will examine the effect of adsorption of small ligands on the atomic and electronic structures of germanene.

3.3.1 Structural properties

In our work we adsorb -H, -CH_3, -C_2H and -CH_2CHCH_2 on germanene. We chose these radicals based on recent synthesized structures [36, 37, 38, 39]. Besides, we have also calculated adsorption of others functionals such as -COOH

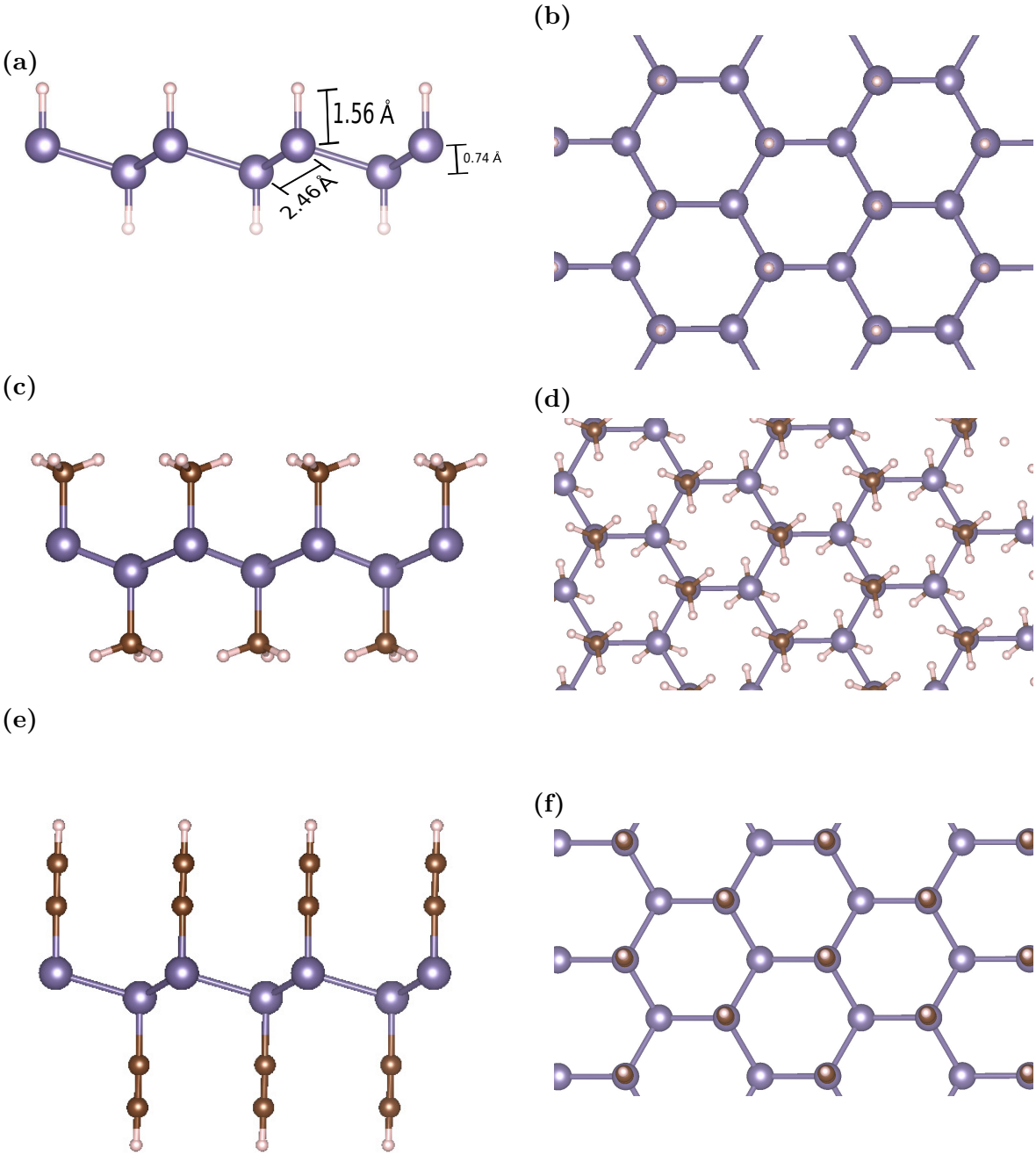

Figure 3.10. Side view of optimized atomic structures: (a) Ge-H , (c) Ge-CH_3 and (e) Ge-C_2H. Top view of optimized atomic structures on (b) Ge-H , (d) Ge-CH_3 and (f) Ge-C_2H. Grey, brown and pink spheres are germanium, carbon and hydrogen atoms, respectively.

We then relax the atomic position and lattice parameters of all hybrid systems. The final optimized structures are shown in Figs. (3.10), (3.11) and (3.12).

As shown in table 3.1, the lattice parameter of Ge-H was 4.08 (Å), with Ge-Ge bond length of 2.46 (Å). The obtained buckling was 0.74 (Å). The structure is symmetric on both sides. The Ge-H bond length Ge-H was 1.56 (Å).

For the Ge-CH_3 the lattice parameter is 4.11 (Å). The buckling is larger compared to previous structure with a value of 0.78 (Å). The ligands lie upright to the germanene

sheet. The distance between germanium atoms and germanium-carbon atoms are 2.48 (Å) and 2.01 (Å), respectively.

Now we analyze the Ge-C_2H structure. The lattice parameter a is 4.15 (Å) as shown in table 3.1. There was a significant increase in the Ge-Ge bond length 2.50 (Å) compared to bare germanene. Due to the fact that this radical has a larger volume than Ge-CH_3 and Ge-H, the buckling is 0.70 (Å).

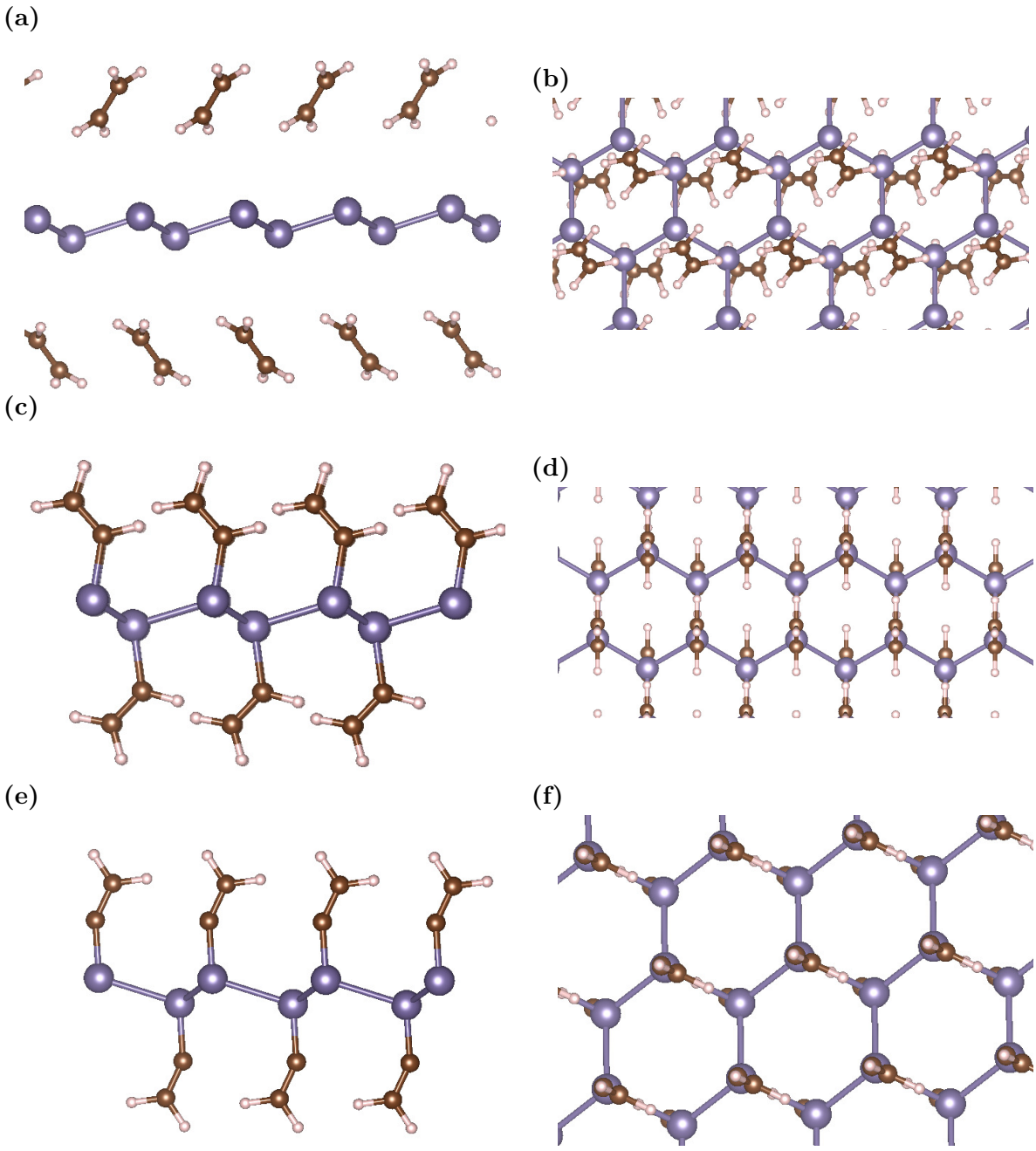

Figure 3.11. Side view of optimized germanium hybrid structures: (a) Ge--CH_2CH_2 , (c) Ge-$CHCH_2$ and (e)Ge-C_2H_2. Top view of optimized atomic structures: (b) Ge--CH_2CH_2 , (d) Ge-$CHCH_2$ and (f) Ge-C_2H_2. Grey, brown and pink spheres are germanium, carbon and hydrogen atoms, respectively.

In addition to C_2H, we also functionalized C_xH_x radicals, with x ranging from 0 to 2 as shown in Fig.(3.11). The optimized structure for Ge--CH_2CH_2 has a lattice parameter of 4.07 (Å), as shown in table 3.1. The Ge-Ge bond length is 2.44 (Å) and the buckling is 0.53 (Å). The bonds between the radical and germanene is 4.82 Å, which is very large. This can be explained noticing that this is a very stable radical and therefore no adsorption of this radical is possible.

For Ge-$CHCH_2$ we find a lattice parameter of 4.24 (Å), the bond length between Ge-Ge was 2.50 (Å) and Ge-C bond length was 1.87 (Å), with buckling of 0.61 (Å).

Finally, the lattice parameter of Ge-C_2H_2 was 4.08 (Å), with Ge-Ge bond length of 2.20 (Å). The calculated buckling was 0.58 (Å).

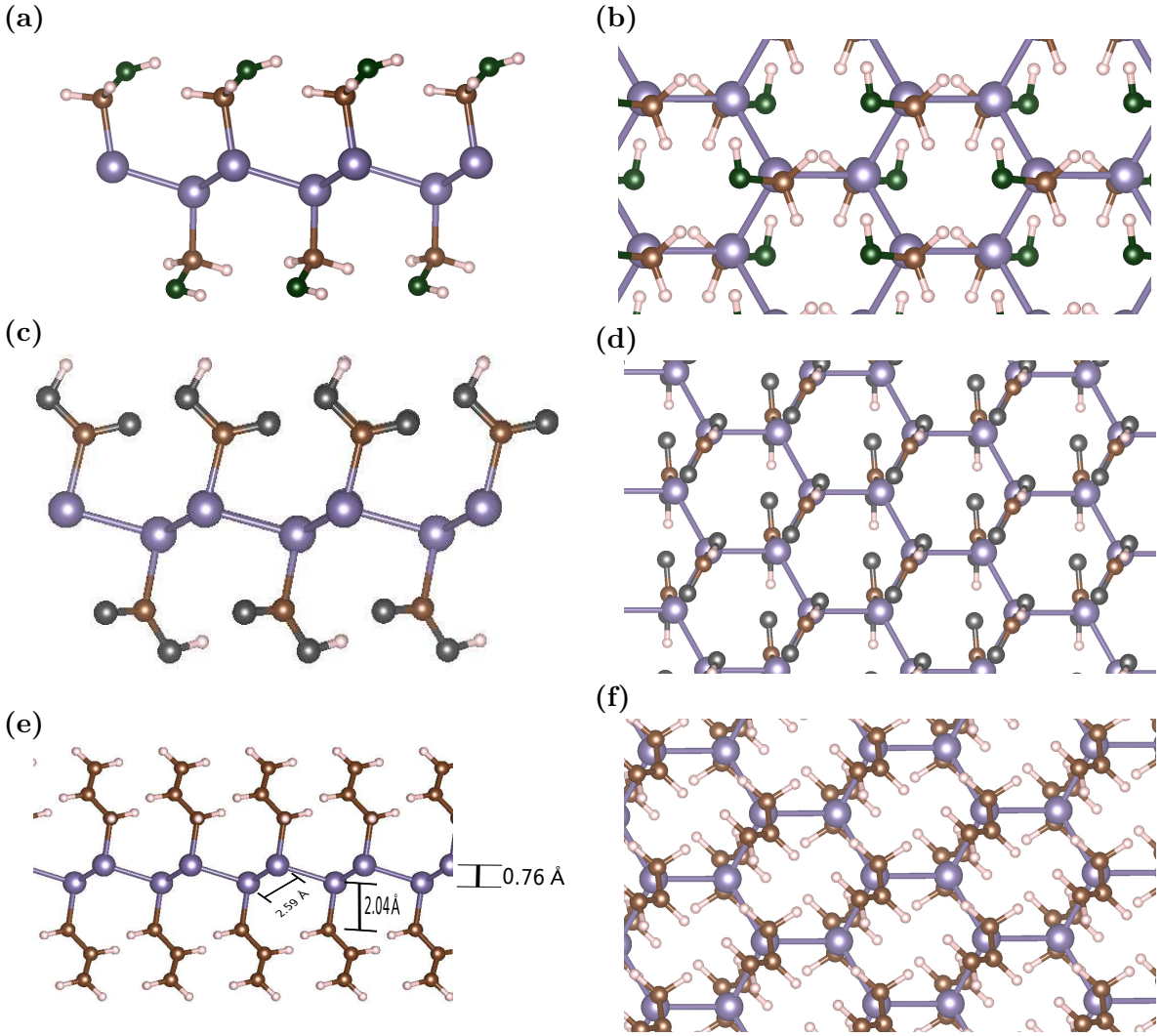

Figure 3.12. Side view of optimized germanium hybrid structures: (a) Ge-CH_2OH , (c) Ge-COOH and (e) Ge-CH_2CHCH_2. Top view of optimized atomic structures: (b) Ge-CH_2OH , (d) Ge-COOH and (f) Ge-CH_2CHCH_2. Grey, brown, green and pink spheres are germanium, carbon, oxygen and hydrogen atoms, respectively.

Ge-CH_2OH had lattice parameter of 4.16 (Å), as displayed in table 3.1. The Ge-Ge bond length is 2.53 (Å) and Ge-C bond length is 2.04 (Å) with buckling of 0.77

(Å).

The lattice parameter of Ge-COOH is 4.20 (Å). The bond length between Ge-Ge is 2.57 (Å) and Ge-C bond length is 2.05 (Å). The ligand adopts a tilted geometry. The buckling is 0.74 (Å).

Ge-CH_2CHCH_2 is the largest ligand investigated in this work, with a lattice parameter of 4.30 (Å). The Ge-Ge distance is 2.59 (Å) with Ge-CH_2CHCH_2 bond length of 2.04 (Å).

	a(Å)	Ge-Ge (Å)	Ge-X (Å)	buckling (Å)	$E_g(eV)$
Ge(germanene)	4.05	2.43	—	0.69	0.023
Ge-CH_2CH_2	4.07	2.44	4.82	0.53	0.02
Ge-H	4.08	2.46	1.56	0.74	0.88;1.51*;1.46[36]
Ge-CH_3	4.11	2.48	2.01	0.78	0.69;1.86[37]
Ge-C_2H	4.15	2.50	1.92	0.70	0.46
Ge-CH_2OH	4.16	2.53	2.04	0.77	0.77
Ge-C_2H_2	4.20	2.54	1.98	0.58	0.75
Ge-COOH	4.20	2.57	2.05	0.74	0.80
Ge-$CHCH_2$	4.24	2.50	1.87	0.61	0.50
Ge-CH_2CHCH_2	4.30	2.59	2.04	0.76	0.41

Table 3.1: Lattice parameters a, Ge-Ge distance, Ge-ligand distance Ge-X, buckling and energy gap E_g of hybrid germanene structures. Values with * imply HSE calculations.

3.3.2 Electronic properties

In this section we discuss the electronic properties of functionalized germanium.

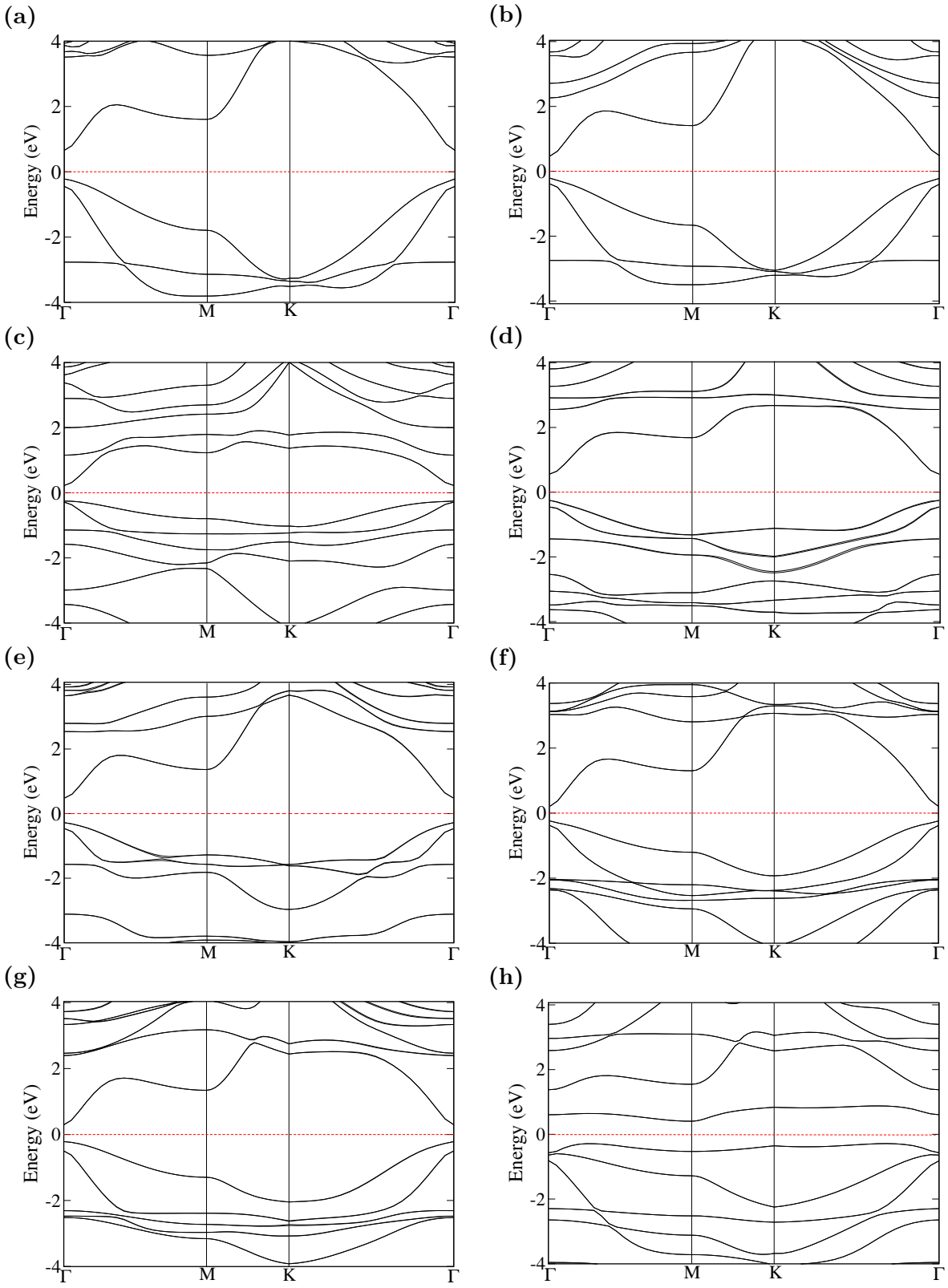

Figure 3.13. Band structures of (a) Ge-H, (b) Ge-CH_3, (c) Ge-CH_2CHCH_2, (d) Ge-COOH, (e) Ge-CH_2OH, (f) Ge-C_2H, (g) Ge-$CHCH_2$ and (h) Ge-C_2H_2. The dashed line denotes the Fermi energy.

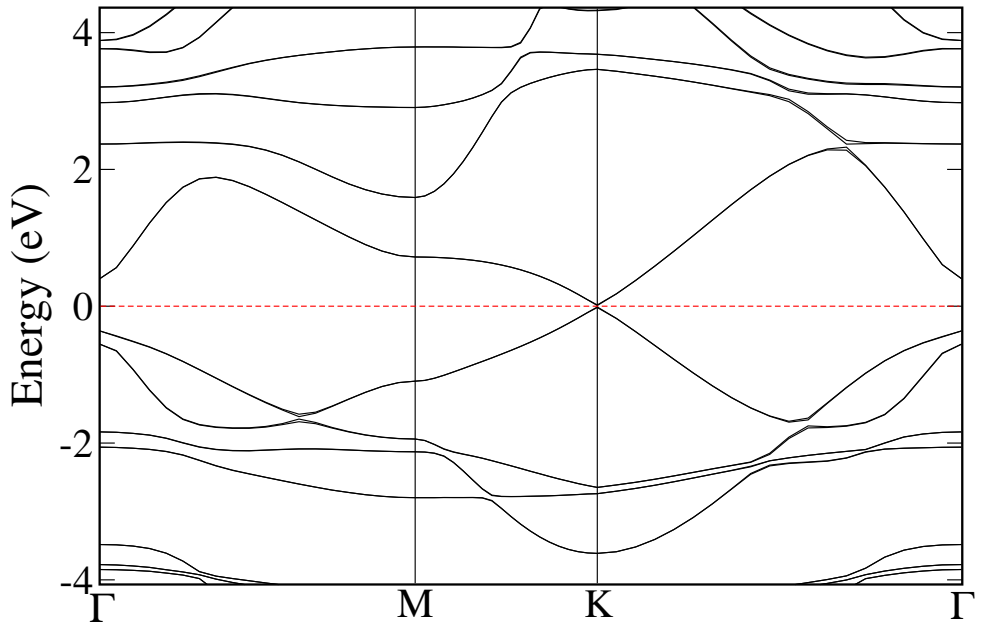

Figure 3.14. Electronic band structures of Ge-CH_2CH_2. The dashed line denotes the Fermi level.

The Ge-H has a gap at Γ point with a value of 0.88 eV . At K point the Dirac cone has disappeared. Ge-CH_3 opened a direct gap of 0.69 eV at Γ point. The Ge-CH_2CHCH_2 has a smaller direct gap than other hybrid systems, with a value of 0.41 eV at point K.

Ge-COOH has a larger direct gap than other hybrid systems, with 0.80 eV at point K and again and the Dirac cone has moved to the Γ point.

Next, we calculated the band structure of Ge-CH_2CH_2. The band structure shows a gap of only 0.02 eV, which is due to germanene, since the interaction between germanium atoms and the ligand is negligible.

For the Ge-CH_2OH system we obtain a direct gap of 0.77 eV at K point. Ge-C_2H and Ge-$CHCH_2$ have a direct gap of 0.46 eV and 0.50 eV at Γ point. In Ge-C_2H_2 the band structure of this material has an indirect gap of 0.75 eV.

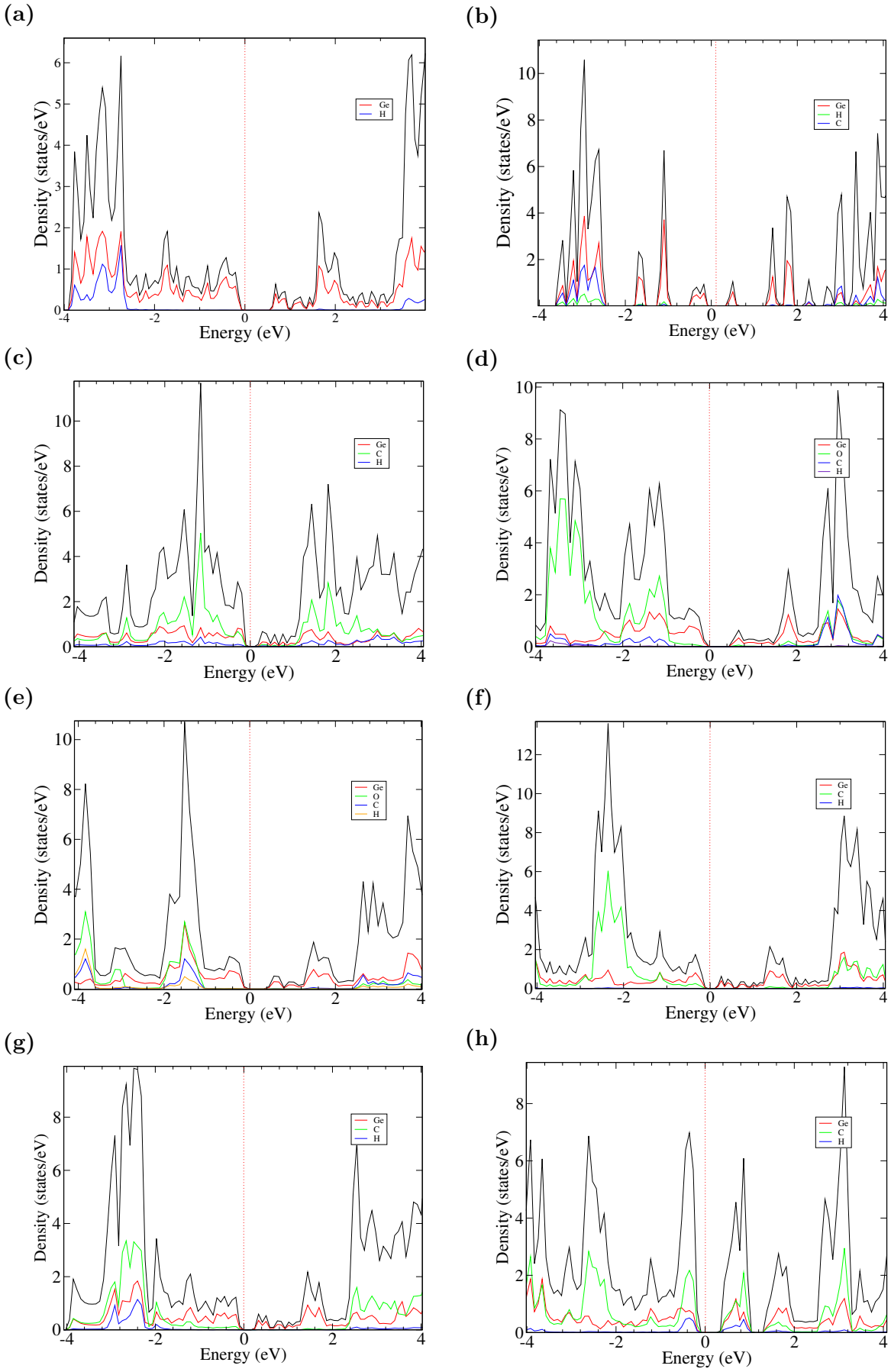

Figure 3.15. Density of States of (a) Ge-H, (b) Ge-CH_3, (c) Ge-CH_2CHCH_2, (d) Ge-COOH, (e) Ge-CH_2OH, (f) Ge-C_2H, (g) Ge-$CHCH_2$ and (h) Ge-C_2H_2. At the origin the Fermi level is fixed

In order to understand the different atomic contributions, we have calculated the total density of states (DOS) and the atom-projected DOS of functionalized germanium layers, as shown in Fig. 3.15. All our calculations, except for Ge-C_2H_2, showed that the biggest contribution to the DOS stems from the germanium atom. For the functionalized radicals that have oxygen in their composition, such as Ge-COOH and Ge-CH_2OH, there was no contribution close to the conduction and valence band.

Note that at point K, the Dirac cone has been eliminated in all systems except for Ge-CH_2CH_2, translating the energy gap to Γ point. The greatest contribution of the bands close to the Fermi level comes from the p orbital. Thus, in the presence of organic ligands, there is a change in the underneath germanium layers, On the other hand, for the Ge-C_2H_2, there was no real chemical adsorption and therefore there was no change in the Dirac cone in the band structure of this material.

3.3.3 Charge density difference

In order to better understand the effect of ligands on the germanium structures, we calculated the charge density difference $\Delta\rho$ defined as:

$$\Delta\rho = \rho^{Ge-X} - \rho^{Ge} - \rho^{X}, \tag{3.3.1}$$

where $\rho^{\mathrm{Ge-X}}$ is the electronic density of the hybrid Ge-X layers, ρ^{Ge} and ρ^{X} are the charge densities of the germanium layers and the ligand, respectively, calculated at fixed atomic positions. The results are shown in Fig. 3.16.

The nature of the chemical bonds presented in the hybrid systems was investigated by the charge density difference between the electronic densities of the adsorbed germanium layers and their constituent systems. Positive (negative) values should correspond to an area of electron density enrichment (depletion). Blue and red regions correspond to positive and negative electronic charge modifications, respectively, between the Ge substrate and the ligands.

As a general feature, charge accumulation on the ligand and charge withdrawal close to the germanium atom are seen. The complex Ge-H shown in Fig. 3.16(a) has a higher electronic density at germanium site and a withdraw of electrons at hydrogen sites.

Upon -H adsorption bonds between hydrogen and germanium atoms are formed. The complex Ge-COOH also shows accumulation of charge at the ligand, oxygen and carbon atoms, while charge is accumulated at the germanium site (see Fig. 3.16 (c)).

The complex Ge-CH_3 shown in Fig. 3.16(b) shows that charge is extracted from germanium after adsorption in the germanium layers. Between C and Ge bonds there is an excess of electrons. Between C and Ge bonds there is a negative charge slightly displaced to the carbons due to its electronegativity greater than that of germanene.

The complex Ge-CH_2OCH_3 also shows accumulation of charge at the ligand, mainly on the oxygen and carbon atoms, while positive charge (withdraw) is accumulated at the germanium site (see Fig. 3.16 (e)). Between C and Ge bonds there is an excess of electrons shifted to carbons.

The complex Ge-CH_2CHCH_2 also shows accumulation of electroni charge at the ligand, more specificcaly on the carbon atoms, while regions close to the germanium are charge depleted. At the germanium site and between C and Ge bonds there is an excess of electrons as it can be seen in Fig. 4.7(d).

For hybrid Ge-CHC_2 and Ge-C_2H_2 we have a similar result, with different intensities due to the additional hydrogen.

In Fig. 3.17 we have Ge-CH_2CH_2 where there was no adsorption so there is no difference in charge density. This is quite interesting, since it reveals that the role of all ligands is to introduce a new function to the germanene by changing its reactivity. Due to the charge accumulation/withdraw in the modified layers, the reactivity of the whole system changes.

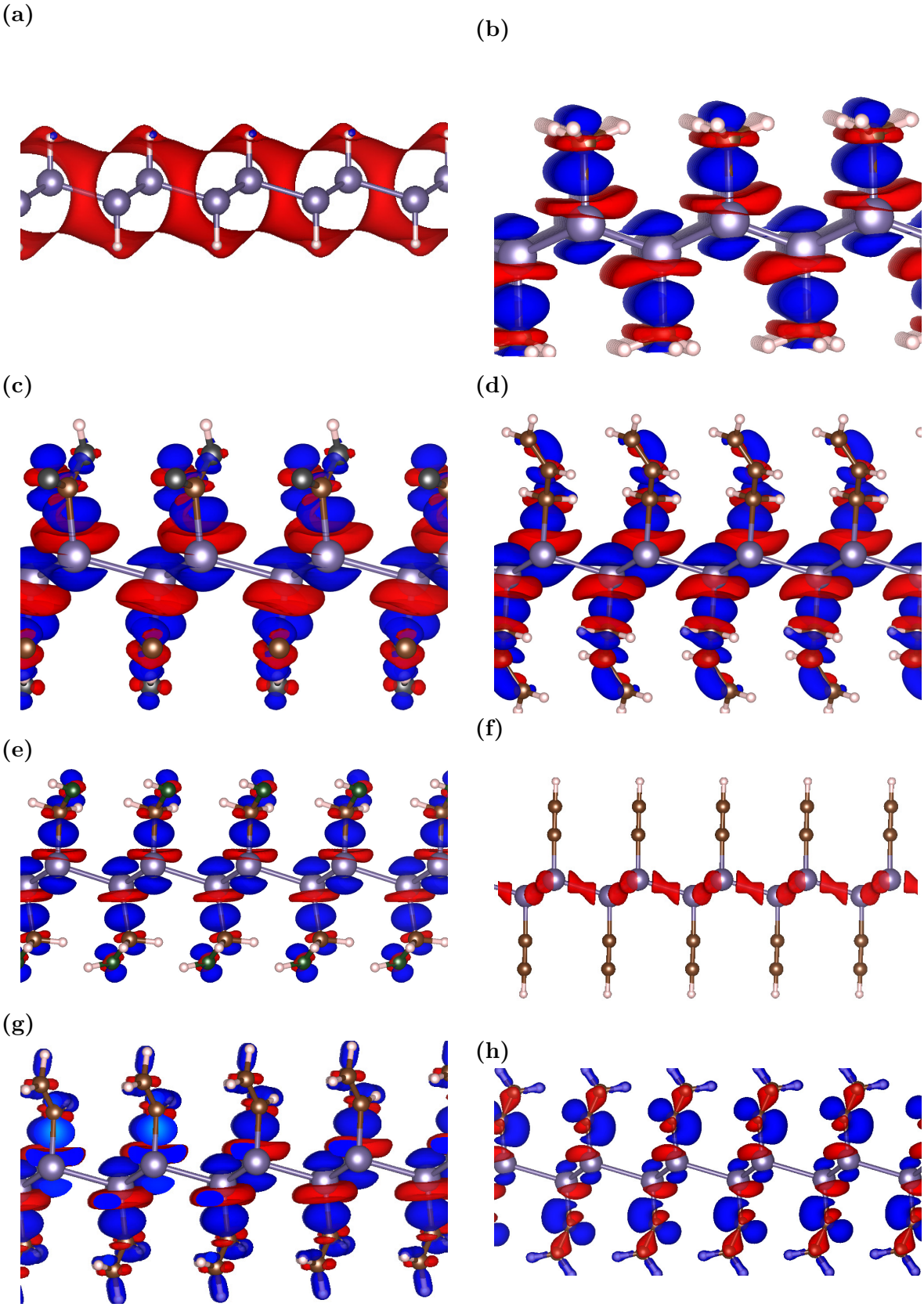

Figure 3.16. Isosurfaces $\Delta\rho$. Negative (positive) charge is shown in red (blue). (a) for Ge-H, (b) for Ge-CH_3, (c) for Ge-COOH, (d) Ge-CH_2CHCH_2, (e) Ge-CH_2OH and (f) C_2H (g) $CHCH_2$ (h) C_2HC_2H

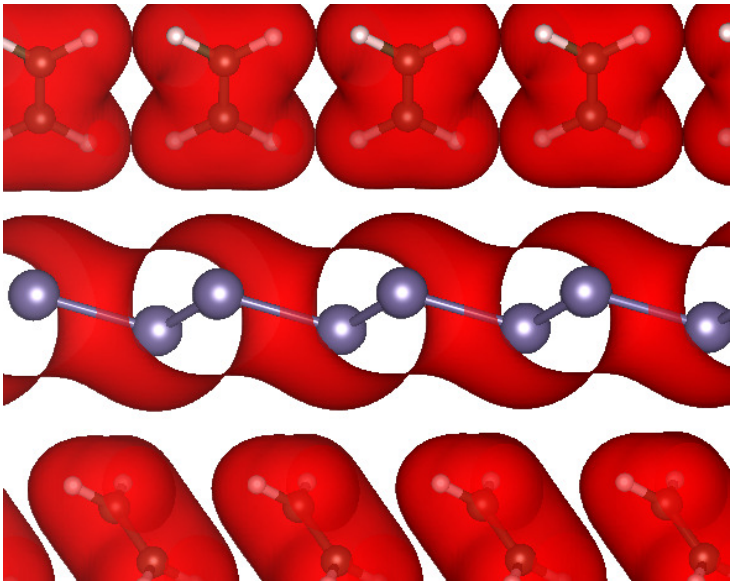

Figure 3.17. Isosurfaces $\Delta\rho$. Negative charge is shown in red from CH_2CH_2

From the discussion above, we can see that the buckling shows little change regardless the ligand as shown in table 3.1. On the other hand, bond lengths between germanium and the ligands show a large variation with the ligand size. All of them are around 2.0 (Å) for carbon and 1.5 (Å) for hydrogen, compliant with the results for the atomic van der Waals Radii [40].

Finally we would like to mention that our results are in good agreement with the ones in the literature for Ge-H and Ge-CH_3 systems regarding structural properties [36, 37]. Additionaly we have calculated the band gap using hybrid functionals (HSE-06). The change in the gap is shown in table 3.1. As we can see the band gap increases due to a different description of the exchange-corrrelation potential.

All functionalized structures that were studied in this work have a band gap. Therefore, adsorption of organic ligands are able to change the electronic properties of germanene which is useful for applications of these systems in electronic devices, especially when searching for new ligands with lower cost.

CHAPTER 4

Defects in germanene

Defects in materials are often studied in science and they are always found in nature, however these defects can cause changes in the properties of the material that can be beneficial in technological applications. We seek to understand the electronic structure of germanene in the presence of several types of defects such as vacancies.

The defects of the type vacancy have a great interest in condensed matter, because the electronic structure and optical properties are very sensitive to the atomic structure of the material. In this chapter, we will explore vacancies in germanene and also nanopores.

4.1 Point defects

In this section we will describe our investigations on germanene in the presence of vacancies, vacancy is the absence of an atom or set of atoms in its lattice structure.

4.1.1 Monovacancy

In our calculations we use a (4x4) unit cell as shown for the initial structure in Fig.(4.1).

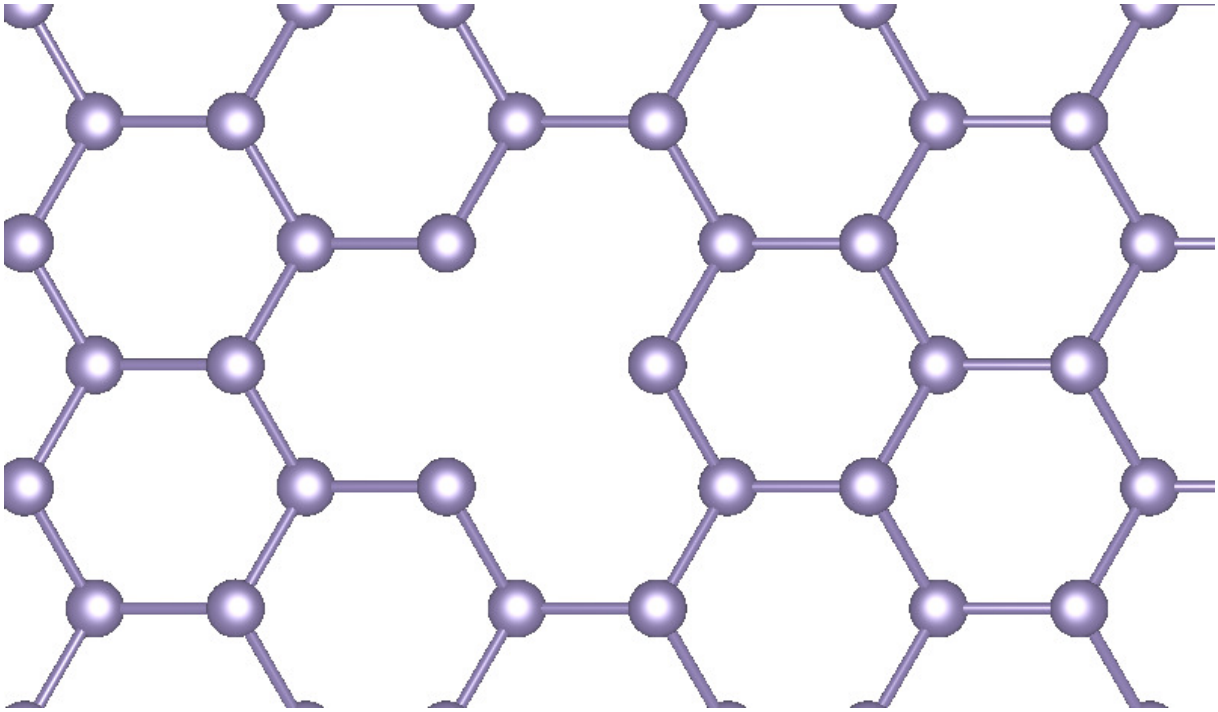

Figure 4.1. Initial structure of a monovacancy

The relaxed structure produces a defect called (555), where pentagons are formed close to the vacancy, as shown in Fig. 4.2.

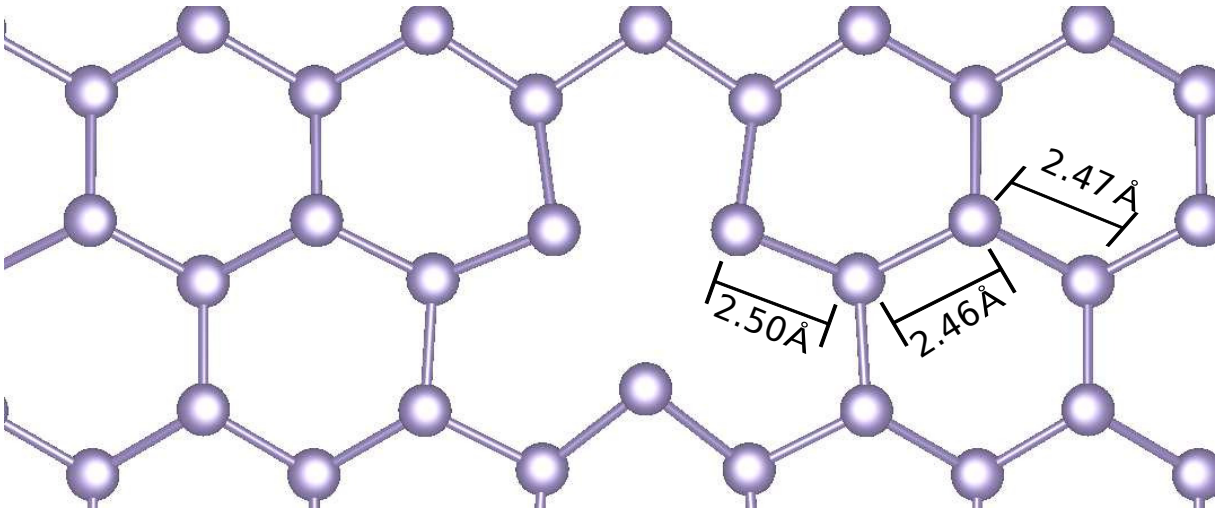

Figure 4.2. Germanene with a monovacancy.

The distance between the first neighbors close to vacancy is 2.50 (Å), to second neighbors 2.46 (Å) and third neighbors onwards 2.47 (Å) as shown in Fig. 4.2. We have calculated the density of states of germanene monovacancy. The system is now metallic, with a large contribution close to the conduction band and valence band of the p orbital, as shown in the Fig.(4.3).

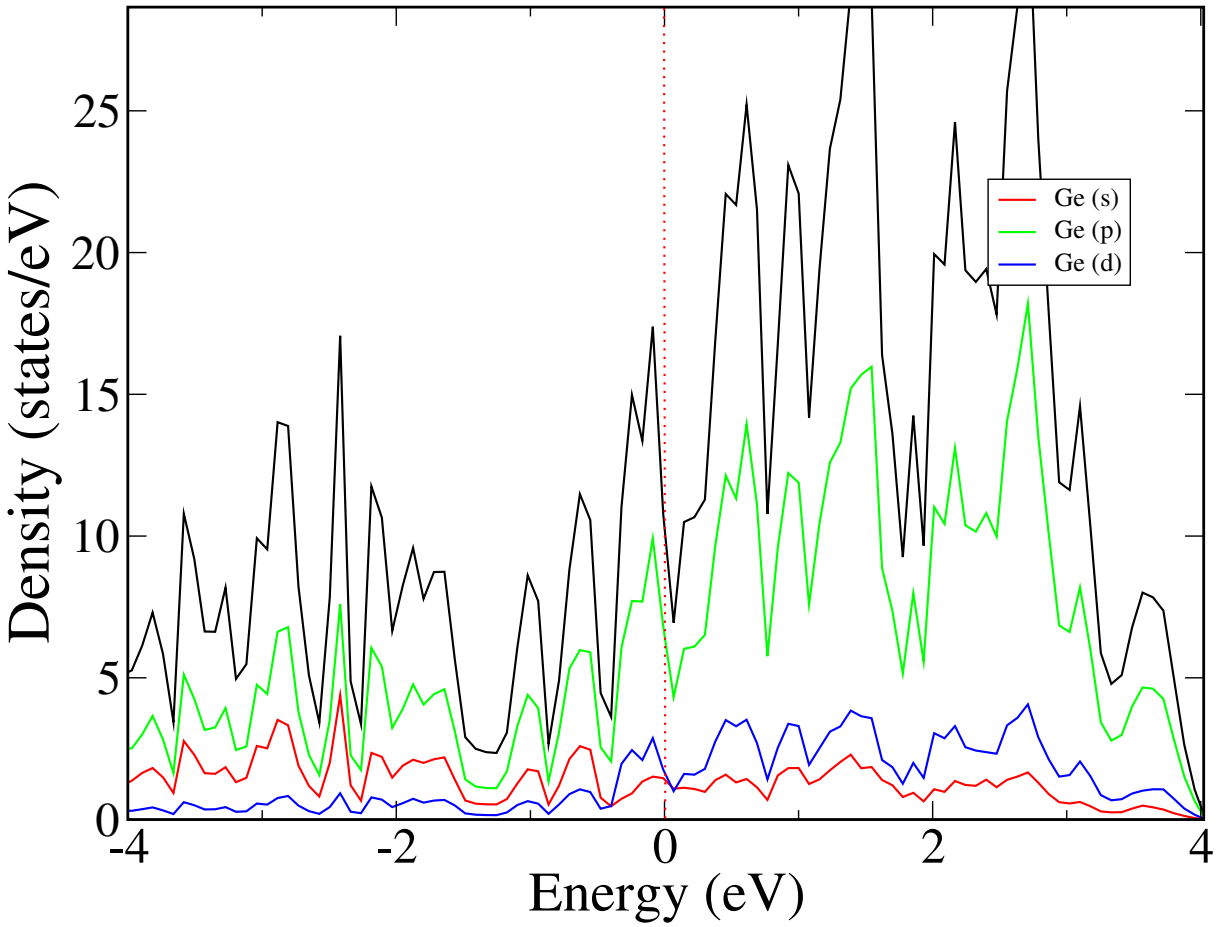

Figure 4.3. Density of states of germanene monovacancy. The Fermi level is set at zero.

4.1.2 Divacancy

In a divacancy there are two germanium atoms missing. There are two possibilities: the divacancy can occur in the same planes or in different planes, as shown in Fig.(4.4).

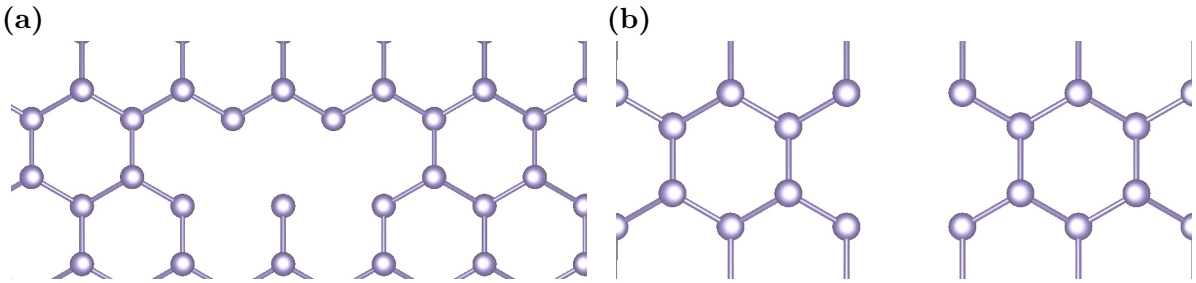

Figure 4.4. (a)Divacancy within the same plane and (b) in different planes.

4.1.3 Divacancy within same layer

The relaxed structure is shown in Fig.(4.5).

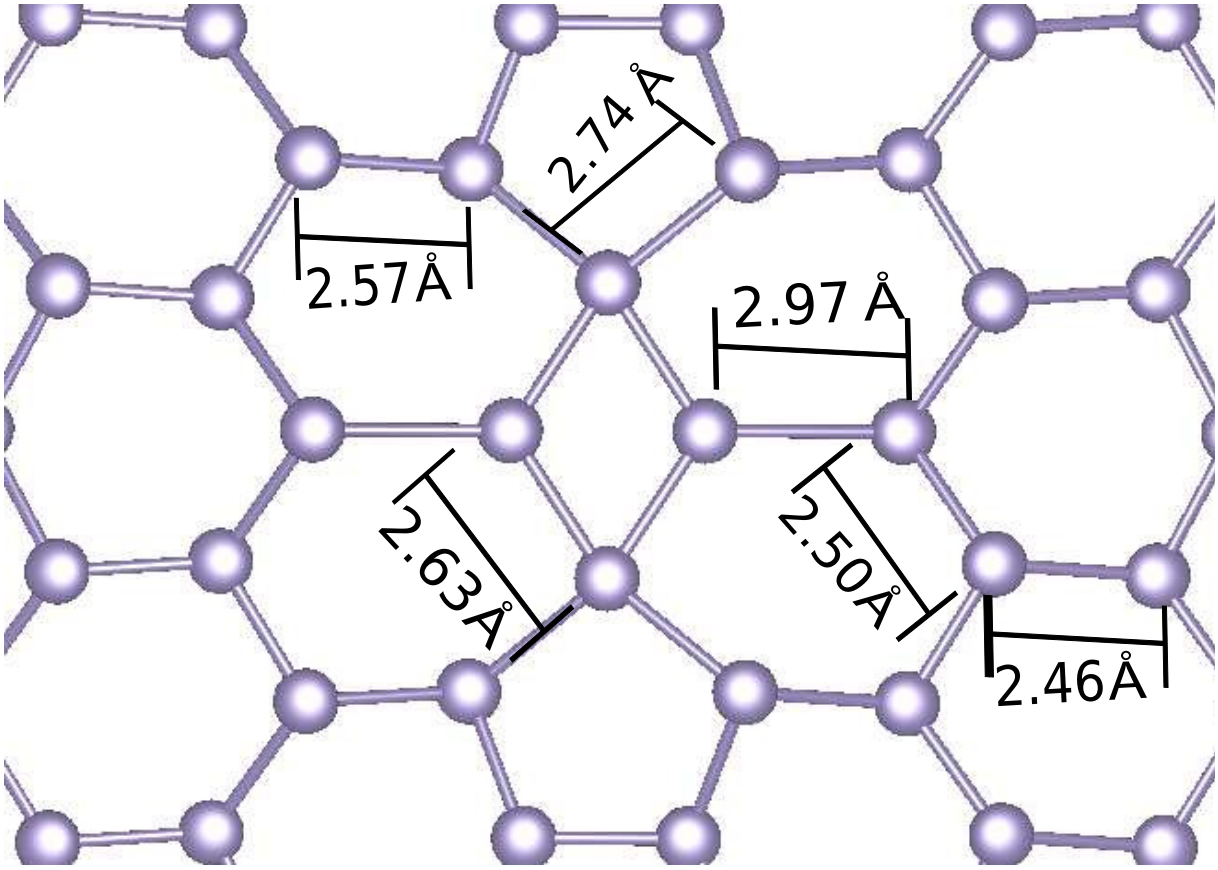

Figure 4.5. Relaxed divacancy within the same plane.

Divacancy wihin the same plane in germanene relaxes the structure for Ge-Ge distances of 2.63 (Å), 2.74 (Å) and 2.50 (Å) as shown in Fig.(4.5).

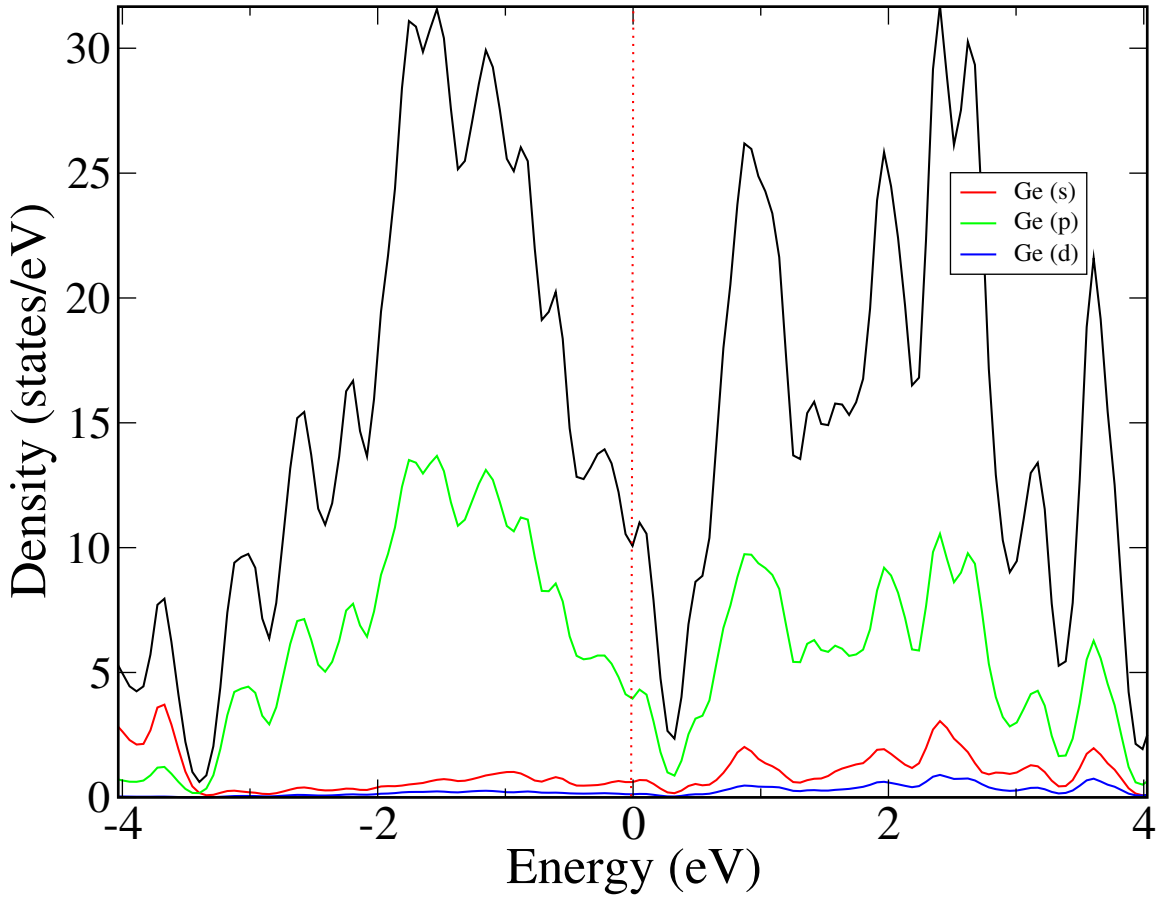

Figure 4.6. Density of states of the divacancy within the same plane. The Fermi level is set at zero.

We calculated the density of states to divacancy within the same plan, We find that the system is metallic with large contribution from the p orbitals.

4.1.4 Divacancy in different layers

For divacancy in different plan the so-called (585) defect is produced, that is, two pentagons and an octagon as shown in Fig.(4.7). Within the pentagon the distances between germanium atoms was 2.44 (Å) and those that form the octagon are 2.57 (Å). Further distances are 2.45 (Å).

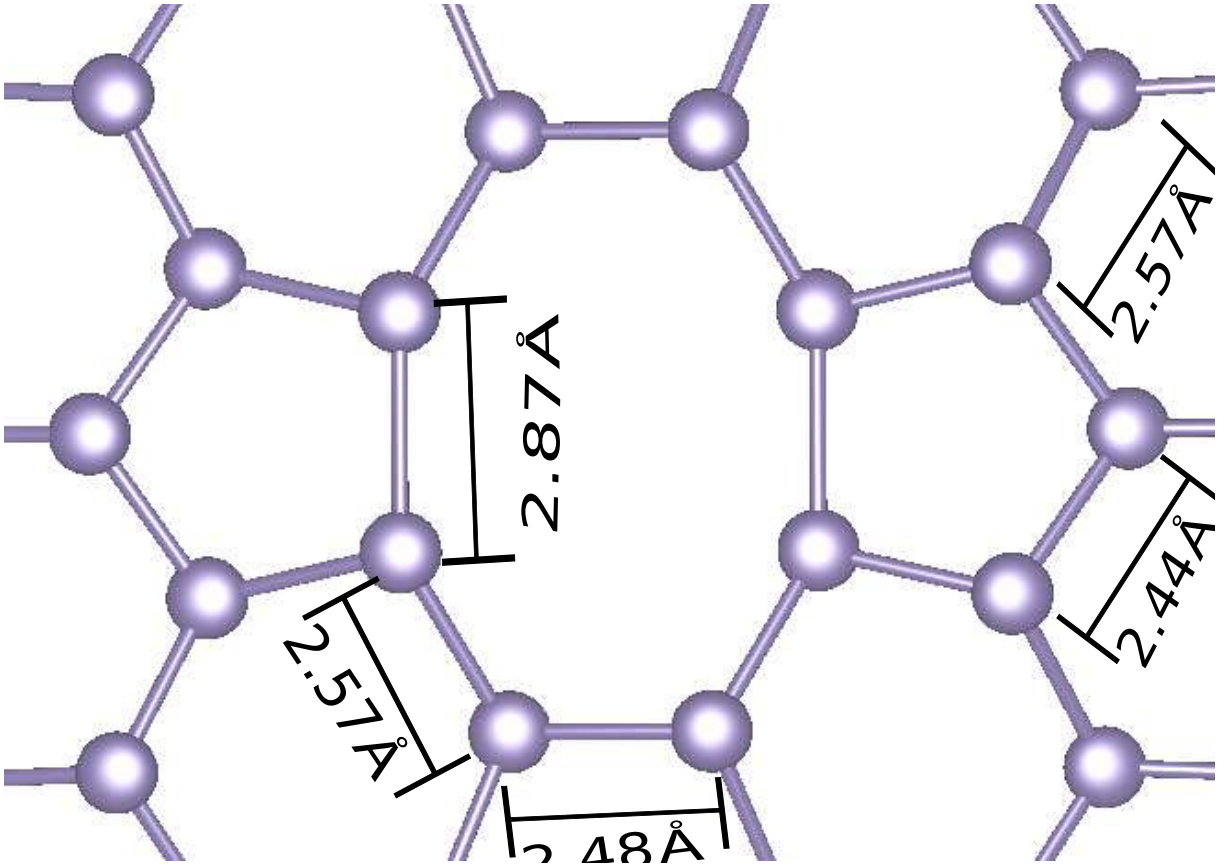

Figure 4.7. Relaxed structure of germanene with Divacancy in different layers.

We calculated the density of states for the divacancies. As shown in Fig.(4.8) we have a metallic character.

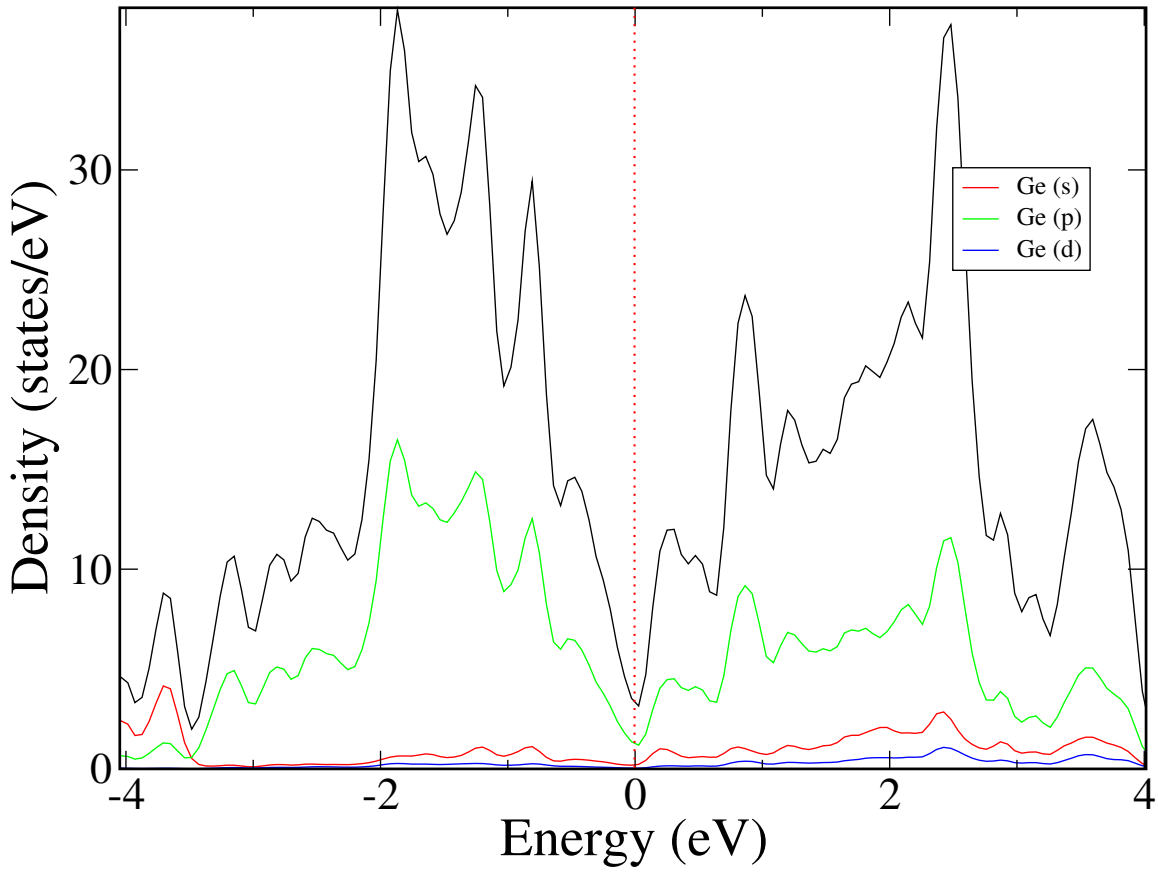

Figure 4.8. Density of states of the divacancy within different planes. The Fermi level is set at zero.

Presence of s, p close to the Fermi level with larger contribution of the p orbitals. Comparing to the monovacancy and divacancy there is change in the behavior of the material.

4.2 Germanene nanopores

Another type of defect that occurs in nature is the presence of pores in the structures. For germanene note that these pores are on the nanometer scale.

4.2.1 Trigonal nanopore

In our calculations for trigonal nanopore we replicate our germanene unit cell to (4x4), produce the trigonal nanopore we remove germanium atoms highlighted as shown in Fig.(4.9), all our calculations made by trigonal nanopore were included spin-orbit coupling.

With the relaxation of the germanene structure with the trigonal nanopore, there was a break in the binding after the relaxation, distancing the atoms by 2.68 (Å), also forming some pentagons with distance between germanium of 2.42 (Å) in the structure as is shown in Fig.(4.10).

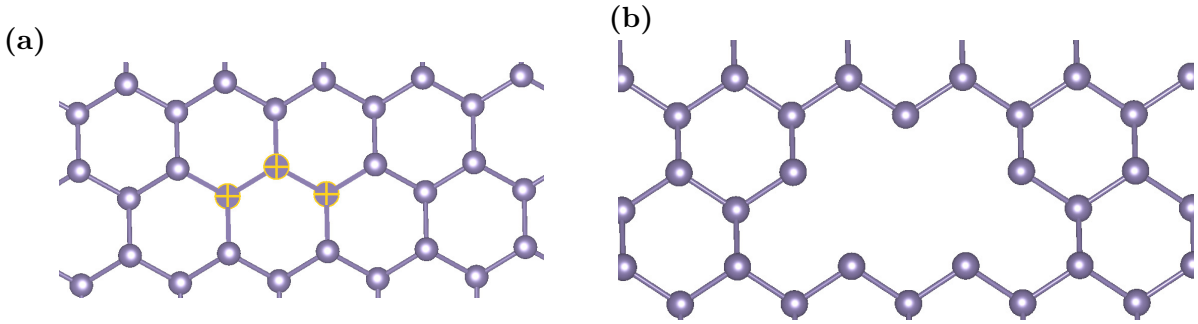

Figure 4.9. (a)Removal of germanium atoms in order to produce a trigonal nanopore in germanene and (b) germanene with trigonal nanopore.

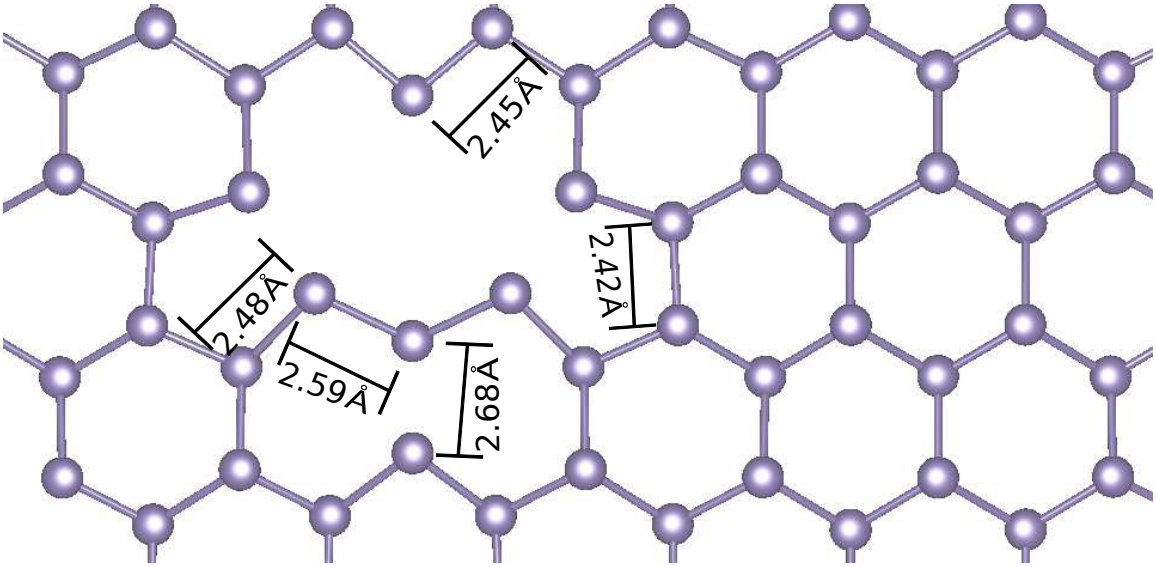

Figure 4.10. Relaxed structure of germanene with trigonal nanopore.

With the triangular type nanopore in the structure, we calculated the density of states as shown the Fig.(4.11) the structure changed the electronic properties of the system, with the insertion of the nanopore the material has a more metallic character than bare germanene, the greater contribution to the p and d orbitals close to the Fermi level

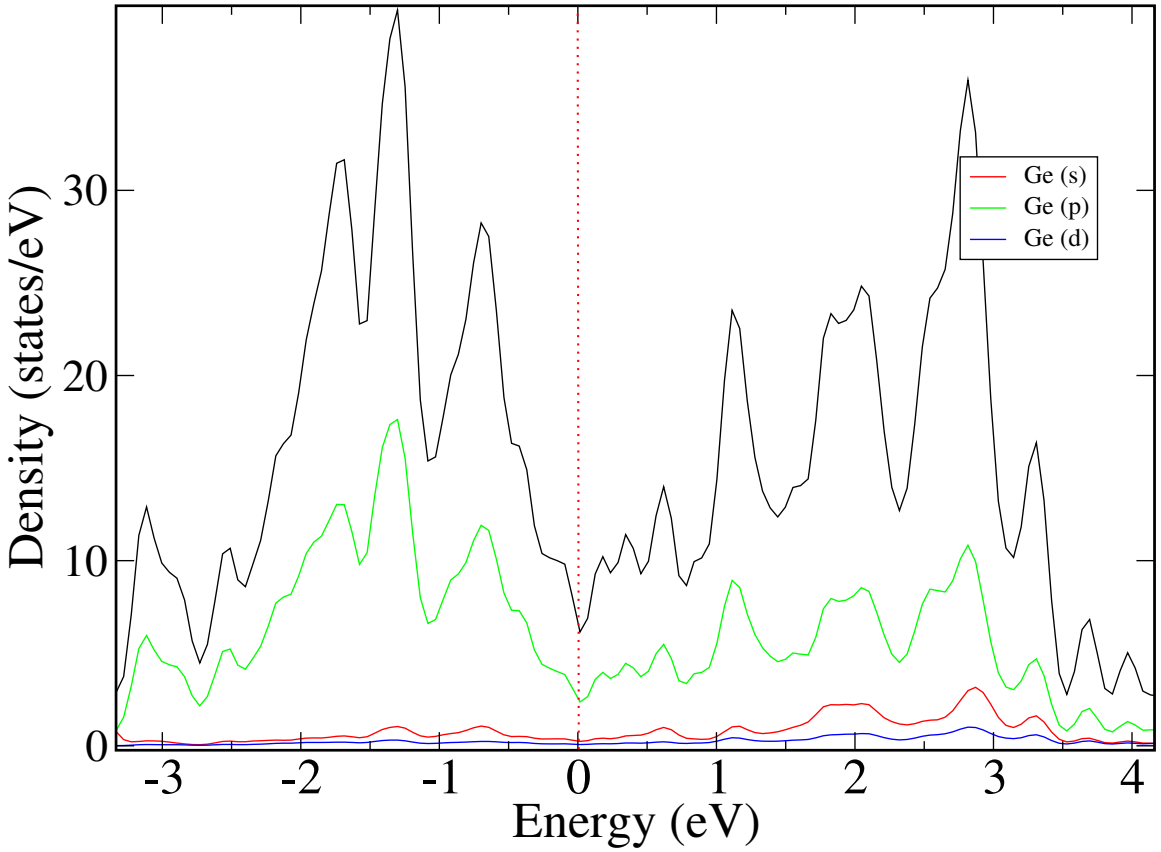

Figure 4.11. Density of states of the trigonal nanopore, at the origin the Fermi level is fixed

4.2.2 Hexagonal nanopores

The hexagonal nanopore consists of the removal of six atoms. We used a (8x8) unit cell, so that we can isolate the nanopore as shown in Fig.(4.12).

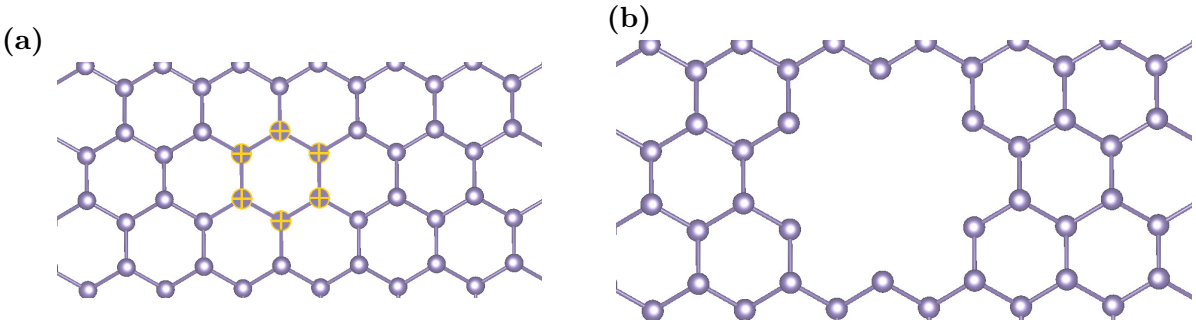

Figure 4.12. (a)Highlighted germanium atoms to produce a hexagonal nanopore in germanene and (b) germanene with hexagonal nanopore.

We calculated the relaxed germanene structure with hexagonal nanopore as shown in Fig.(4.13),

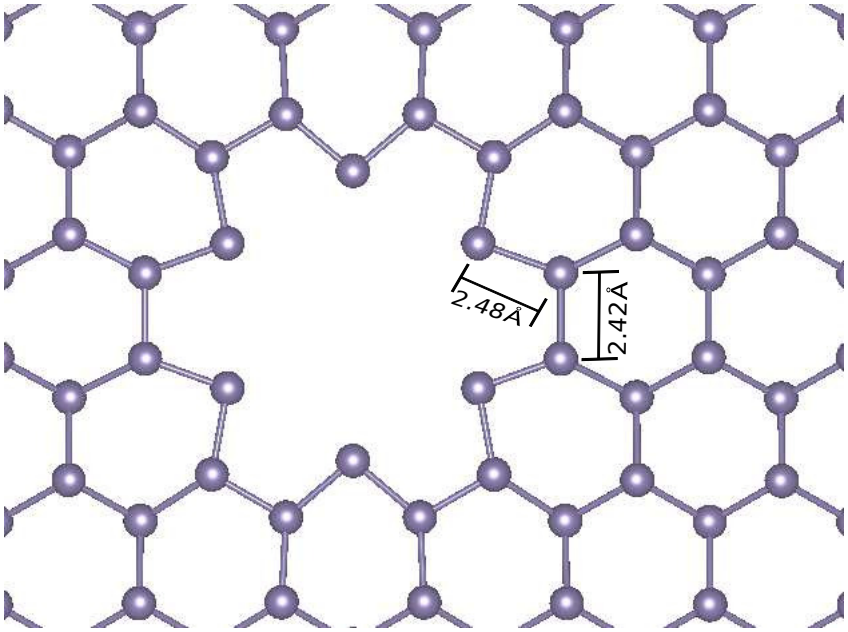

Figure 4.13. Relaxed structure of germanene with hexagonal nanopore.

The first neighboring germanium atoms have bond lengths of 2.48 (Å), the second neighbors of 2.42 (Å) and the third neighbours of 2.43 (Å). Further atoms have a bond length distance that converges to 2.44 (Å).

We calculated the density of states of the hexagonal nanopore germanene. This pore is metallic, as shown in Fig.(4.14). We can see the presence of s and p orbitals at the Fermi level, mainly p_z orbitals.

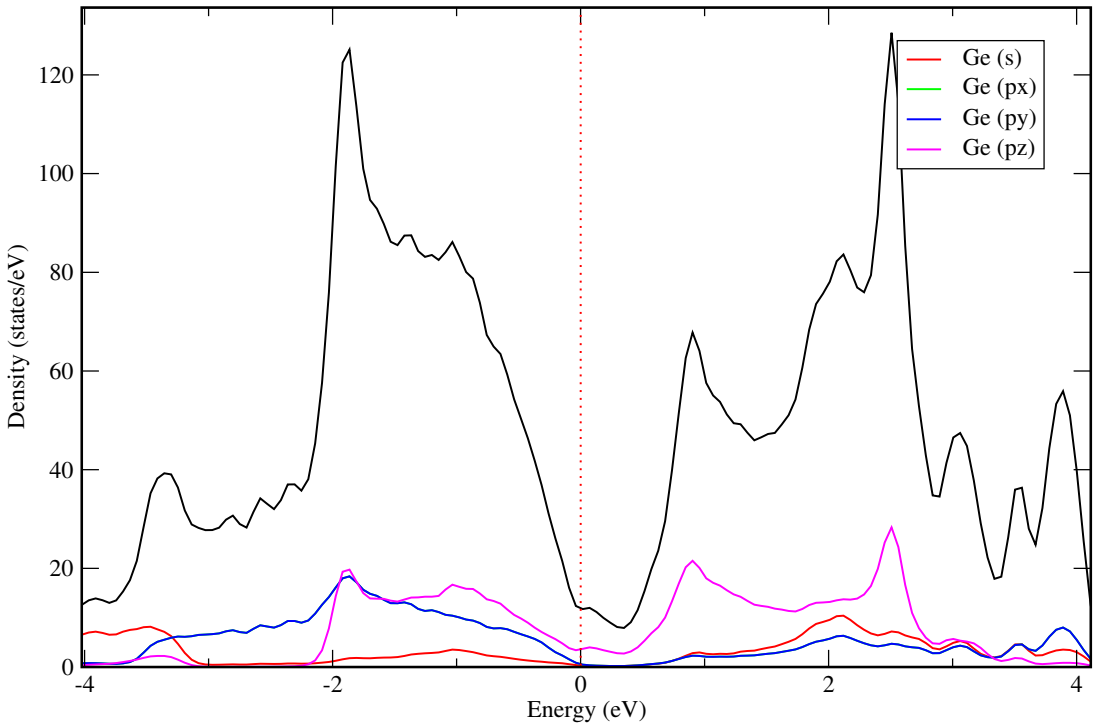

Figure 4.14. Density of states of the hexagonal germenene nanopore. The Fermi level is set at zero.

Our results are in very good agreement with the ones in previous results, such as the defects monovacancy, vacancy type (555), (585) [41, 42]. As a perspective we plan to calculate the functionalization of the pores investigated here in order to undestand how they behave in contact with the environment.

CHAPTER 5

Conclusions and perspectives

Germanene has been recently synthesized to create hybrid layers upon adsorption of organic ligands. It has been shown that modified germanium were stable hybrid materials and with tunable optical properties [3]. Although bare germanium layers have been extensively investigated, functionalized layers with organic molecules has received less attention. For example, several aspects of electronic and optical properties of organic ligand adsorbed germanium layers remained little explored.

In this work we have performed density-functional theory calculations of germanene functionalized with organics groups in order to clarify several aspects regarding ligand-germanene interaction, mainly focusing on the electronic properties of these hybrid materials. Additionally we have investigated germanene containing point and larger structural defects, such as nanopores.

Our results for the ligand adsorbed structures show that the functionalized layers have a sizeable gap which depend on the size and reacitivity of the ligand. Our findings of a finite gap shows open a path for rational design of nanostructures. Our results with vacancies and nanopores show that that a structural modification of the lattice leads to changes in the electronic structure of the material. This can be of great interest since new porous nanostructures have potential applications in new sensors, which could reduce costs for bio and organic molecules detection. Starting from the pores investigated in this work, we could envisage the adsorption of gases and biomolecules on the germanium layers.

As a perspective, we plan to calculate the functionalization of the pores investigated here in order to undestand how they behave in contact with the environment. In a future work to calculate the dynamics of biomolecules passing through different pores.

Finally, we should mention that our results open the path for future investigations on bare and functionalized germanene. The interaction of small molecules with the surface and the germanene pores could be a path for the development of new solid state devices, which are more robust and stable with potential applications in optoelectronic devices.

Bibliography

[1] NOVOSELOV, K. et al. Carrier multiplication in graphene. **Science**, v. 306, p. 666, 2004. Quoted on the page 11.

[2] GEIM, A. K.; NOVOSELOV, K. S. The rise of graphene. **Nature Materials**, v. 6, p. 183, 2007. Quoted on the page 11.

[3] JIANG, S. et al. Improving the stability and optical properties of germanane via one-step covalent methyl-termination. **Nature Communications**, v. 5, p. 3389–33394, 2014. Quoted 2 times on pages 11 e 54.

[4] REN, Y.; QIAO, Z.; NIU, Q. Topological phases in two-dimensional materials: a review. **Rep. Prog. Phys.**, v. 79, p. 066501, 2016. Quoted on the page 11.

[5] ABRISHAMI, M. S.; PEDRAM, M.; NAZARIAN, S. **CSM-NN: Current Source Model Based Logic Circuit Simulation – A Neural Network Approach**. 2020. Quoted on the page 11.

[6] BORN, M. Born-oppenheimer approximation. **Ann. Phys**, v. 84, p. 457–484, 1927. Quoted on the page 13.

[7] HOHENBERG, P.; KOHN, W. Inhomogeneous electron gas. **Phys. Rev.**, American Physical Society, v. 136, p. B864–B871, Nov 1964. Quoted on the page 14.

[8] COULSON, C. A.; MARCH, N. H. Momenta in atoms using the thomas-fermi method. **Proceedings of the Physical Society. Section A**, v. 63, n. 4, p. 367–374, apr 1950. Quoted on the page 14.

[9] FERMI, E. Statistical method to determine some properties of atoms. **Rendiconti Lincei**, v. 6, p. 602–607, 1927. Quoted on the page 14.

[10] KOHN, W.; SHAM, L. J. Self-consistent equations including exchange and correlation effects. **Phys. Rev.**, American Physical Society, v. 140, p. A1133–A1138, Nov 1965. Quoted 2 times on pages 16 e 19.

[11] CEPERLEY, D. M.; ALDER, B. J. Ground state of the electron gas by a stochastic method. **Phys. Rev. Lett.**, American Physical Society, v. 45, p. 566–569, Aug 1980. Quoted on the page 19.

[12] PERDEW, J. P.; ZUNGER, A. Self-interaction correction to density-functional approximations for many-electron systems. **Phys. Rev. B**, American Physical Society, v. 23, p. 5048–5079, May 1981. Quoted on the page 19.

[13] YAKOVKIN, I. N.; DOWBEN, P. A. THE PROBLEM OF THE BAND GAP IN LDA CALCULATIONS. **Surface Review and Letters**, World Scientific Pub Co Pte Lt, v. 14, n. 03, p. 481–487, 2007. Quoted on the page 20.

[14] FIOLHAIS FERNANDO NOGUEIRA, M. A. M. C. **A primer in density functional theory**. 1st edition.. ed. [S.l.]: Springer, 2010. (Lecture Notes in Physics). ISBN 9783642057045,3642057047. Quoted on the page 20.

[15] BECKE, A. D. Density-functional exchange-energy approximation with correct asymptotic behavior. **Phys. Rev. A**, American Physical Society, v. 38, p. 3098–3100, Sep 1988. Quoted on the page 20.

[16] PERDEW, J. P. Density-functional approximation for the correlation energy of the inhomogeneous electron gas. **Phys. Rev. B**, American Physical Society, v. 33, p. 8822–8824, Jun 1986. Quoted on the page 20.

[17] PERDEW, J. P.; BURKE, K.; ERNZERHOF, M. Generalized gradient approximation made simple. **Phys. Rev. Lett.**, American Physical Society, v. 77, p. 3865–3868, Oct 1996. Quoted 2 times on pages 20 e 24.

[18] BECKE, A. D. A new mixing of hartree–fock and local density-functional theories. **The Journal of Chemical Physics**, v. 98, n. 2, p. 1372–1377, 1993. Quoted on the page 21.

[19] LEE, C.; YANG, W.; PARR, R. G. Development of the colle-salvetti correlation-energy formula into a functional of the electron density. **Phys. Rev. B**, v. 37, p. 785–789, 1988. Quoted on the page 21.

[20] PERDEW, J. P.; ERNZERHOF, M.; BURKE, K. Rationale for mixing exact exchange with density functional approximations. **The Journal of Chemical Physics**, v. 105, n. 22, p. 9982–9985, 1996. Quoted on the page 21.

[21] ZHAO, Y.; TRUHLAR, D. G. The m06 suite of density functionals for main group thermochemistry, thermochemical kinetics, noncovalent interactions, excited states, and transition elements: two new functionals and systematic testing of four m06-class functionals and 12 other functionals. **Theoretical Chemistry Accounts**, Springer Science and Business Media LLC, v. 120, n. 1-3, p. 215–241, 2007. Quoted on the page 21.

[22] HEYD, J.; SCUSERIA, G. E.; ERNZERHOF, M. Hybrid functionals based on a screened coulomb potential. **The Journal of Chemical Physics**, v. 118, n. 18, p. 8207–8215, 2003. Quoted on the page 21.

[23] HAMANN, D. R.; SCHLÜTER, M.; CHIANG, C. Norm-conserving pseudopotentials. **Phys. Rev. Lett.**, American Physical Society, v. 43, p. 1494–1497, Nov 1979. Quoted on the page 22.

[24] VANDERBILT, D. Soft self-consistent pseudopotentials in a generalized eigenvalue formalism. **Phys. Rev. B**, American Physical Society, v. 41, p. 7892–7895, Apr 1990. Quoted on the page 22.

[25] KRESSE, G.; HAFNER, J. Norm-conserving and ultrasoft pseudopotentials for first-row and transition elements. **Journal of Physics Condensed Matter**, IOP Publishing, v. 6, n. 40, p. 8245–8257, oct 1994. Quoted on the page 22.

[26] KRESSE, G.; JOUBERT, D. From ultrasoft pseudopotentials to the projector augmented-wave method. **Phys. Rev. B**, American Physical Society, v. 59, p. 1758–1775, Jan 1999. Quoted 2 times on pages 22 e 24.

[27] BLÖCHL, P. E. Projector augmented-wave method. **Phys. Rev. B**, American Physical Society, v. 50, p. 17953–17979, Dec 1994. Quoted 2 times on pages 22 e 24.

[28] KRESSE, G.; HAFNER, J. Norm-conserving and ultrasoft pseudopotentials for first-row and transition elements. **Journal of Physics: Condensed Matter**, IOP Publishing, v. 6, n. 40, p. 8245–8257, oct 1994. Quoted on the page 22.

[29] KRESSE, G.; FURTHMüLLER, J. Efficiency of ab-initio total energy calculations for metals and semiconductors using a plane-wave basis set. **Computational Materials Science**, v. 6, n. 1, p. 15 – 50, 1996. Quoted on the page 24.

[30] ASHCROFT, N. D. M. N. W. W. A. **Solid State Physics**. 1. ed. [S.l.]: Brooks Cole, 1976. (Solid State Physics). ISBN 0030839939,9780030839931. Quoted on the page 27.

[31] DÁVILA, M. E. et al. Germanene: a novel two-dimensional germanium allotrope akin to graphene and silicene. **New Journal of Physics**, IOP Publishing, v. 16, n. 9, p. 095002, sep 2014. Quoted on the page 27.

[32] LIU, C.-C.; FENG, W.; YAO, Y. Quantum spin hall effect in silicene and two-dimensional germanium. **Phys. Rev. Lett.**, American Physical Society, v. 107, p. 076802, Aug 2011. Quoted 2 times on pages 29 e 31.

[33] ACUN, A. et al. Germanene: the germanium analogue of graphene. **Journal of Physics: Condensed Matter**, IOP Publishing, v. 27, n. 44, p. 443002, oct 2015. Quoted on the page 29.

[34] LIU, C.-C.; JIANG, H.; YAO, Y. Low-energy effective hamiltonian involving spin-orbit coupling in silicene and two-dimensional germanium and tin. **Phys. Rev. B**, American Physical Society, v. 84, p. 195430, Nov 2011. Quoted on the page 31.

[35] NI, Z. et al. Tunable bandgap in silicene and germanene. **Nano Letters**, v. 12, n. 1, p. 113–118, 2012. Quoted on the page 31.

[36] BIANCO, E. Stability and exfoliation of germanane: A germanium graphane analogue. **ACS Nano**, 2013. Quoted 3 times on pages 31, 35 e 42.

[37] JIANG, S. et al. Improving the stability and optical properties of germanane via one-step covalent methyl-termination. **Nature Communications**, v. 5, n. 1, p. 3389, 2014. ISSN 2041-1723. Quoted 3 times on pages 31, 35 e 42.

[38] JIANG, S. **Covalent Functionalization of Germanane**. Tese (Doutorado), 2016. Quoted on the page 31.

[39] LIU, N. et al. Recent progress on germanene and functionalized germanene: Preparation, characterizations, applications, and challenges. **Small**, v. 15, n. 32, p. 1805147. Quoted on the page 31.

[40] BONDI, A. Van der waals volumes and radii. **The Journal of Physical Chemistry**, 1964. Quoted on the page 42.

[41] PADILHA, J. E.; PONTES, R. B. Electronic and transport properties of structural defects in monolayer germanene: An ab initio investigation. **Solid State Communications**, v. 225, p. 38 – 43, 2016. ISSN 0038-1098. Quoted on the page 53.

[42] MONSHI, M.; AGHAEI, S.; CALIZO, I. Doping and defect-induced germanene: A superior media for sensing h2s, so2, and co2 gas molecules. **Surface Science**, v. 665, p. 96 – 102, 2017. ISSN 0039-6028. Quoted on the page 53.